Microscopic theory of anisotropic organic cavity exciton polaritons

Hashem Zoubi and G. C. La Rocca
Scuola Normale Superiore and INFM, Piazza dei Cavalieri 7, 56126 Pisa, Italy
(Received 4 November 2004; revised manuscript received 24 January 2005; published 17 June 2005)

We consider crystalline organic microcavities in the strong coupling regime. Using a microscopic theory to describe the Frenkel excitons and their coupling to the cavity photon modes, we derive the cavity exciton-polariton dispersion relations and quantum states, for the two cases of anisotropic organic crystals with one and two molecules per unit cell. In the most general case, the cavity exciton polaritons are a coherent superposition of both Davydov exciton branches and of both cavity mode polarizations. The polarization mixing, which occurs also in the case of a single molecule per unit cell, is in contrast to the case of typical inorganic semiconductor cavities in which TM and TE polarizations do not mix. We derive the transmission, reflection, and absorption coefficients for organic cavities by applying the quasimode approximation for high quality cavities. The crossed polarized spectra, e.g., the TM polarized reflected light for TE polarized incident light, clearly show the optical anisotropy of organic microcavities in the regime of strong coupling.

DOI: 10.1103/PhysRevB.71.235316 PACS number(s): 71.36.+c, 71.35.Cc, 78.40.Me, 78.66.Qn

I. INTRODUCTION

Recently there has been much interest in organic and inorganic microcavities, for their ability to control the coupling between photons and electronic excitations.[1] In the strong coupling regime, where the photon-exciton interaction is larger than the exciton and photon damping rates, the cavity photons and the excitons are coherently coupled to produce the system eigenmodes which are the cavity exciton polaritons.[2] The polariton dispersion relation splits into two branches which are separated by the Rabi splitting frequency, which is proportional to the transition dipole moment. The exciton polaritons in inorganic semiconductor microcavities have been much investigated both theoretically and experimentally.[3] In typical quantum-well microcavities, the coupling between the Wannier-Mott excitons and the cavity photons yields Rabi splitting values of the order of 10 meV.

The large oscillator strength of the organic materials makes the use of organic microcavities more attractive. The strong coupling between the Frenkel excitons in organic materials and the cavity photons results in a Rabi splitting which is easily an order of magnitude larger than that of inorganic microcavities.[4] In particular, a strong coupling regime has been observed in an organic microcavity containing *J* aggregates of cyanine dye,[5] which have an absorption linewidth of about 40 meV, where the Rabi splitting is between 80 and 300 meV, at room temperature.[6] Such materials are disordered, but the case of crystalline organic media is also of great current interest.[7]

In this paper, we study the Frenkel-exciton polaritons of an organic microcavity in the strong coupling regime and their linear optics spectra on the basis of the microscopic theory.[8] There are only a few previous works on crystalline organic microcavities. M. Litinskaia *et al.*[9] have investigated such system in the framework of the macroscopical approach based on the use of the dielectric tensor, and have derived the polariton dispersion equations for one or two molecules per unit cell in the case in which the molecular transition dipole moments are parallel to the microcavity plane. At the same time, Balagurov and one of us[10] have calculated the linear optics spectra of such system using a phenomenological uniaxial dielectric tensor appropriate for the case of one molecule per unit cell and a (4×4) transfer matrix formalism which allows for the polarization mixing.[11] The present *microscopic* theory not only recovers all those results, but also includes the most general case of two molecules per unit cell with general dipole orientations. In particular, in the latter case, four cavity polariton branches are expected with a significant mixing of both Davydov exciton branches when the Rabi splitting is comparable or larger than the Davydov splitting.[12]

In order to develop the microscopic theory, we consider the simplest possible model describing the physically relevant features of a crystalline organic microcavity. The optical confinement in the microcavity is provided by two parallel mirrors at a distance of the order of an optical wavelength. At the center of the microcavity is placed a slab of the organic crystal of width small compared to an optical wavelength, made of monolayers parallel to the microcavity planes. The organic crystal is composed of molecules which are all chemically identical and have inversion symmetry. For the case of two molecules per unit cell, they differ only for the orientation of their transition dipole moments. Initially, for the purpose of calculating the cavity polariton dispersion curves, the mirrors are assumed to be perfect and no dissipation mechanism is included. Then, in order to calculate the linear optics spectra of the microcavity, the quasimode approach is used to couple the cavity polaritons to the external photons and the exciton nonradiative damping is also included. Our results will be illustrated showing for several cases plots of the cavity polariton dispersion curves as well as of the transmission, reflection, and absorption spectra in the different polarizations.

The paper is organized as follows. In Sec. II the cavity modes are introduced. The Frenkel excitons in an anisotropic crystal slab are described in Sec. III. In Sec. IV the corresponding organic cavity exciton polaritons are studied. The organic cavity transmission, reflection, and absorption spectra are calculated in Sec. V. Our conclusions are presented in Sec. VI.

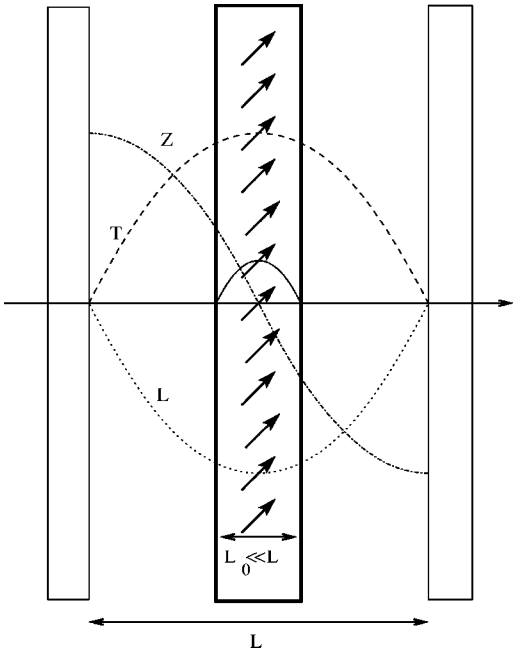

FIG. 1. A molecular crystal slab of width L_0 is located between the cavity mirrors which are separated by distance L. The L, T, and Z components of the $m=1$ cavity modes and the first exciton mode are plotted.

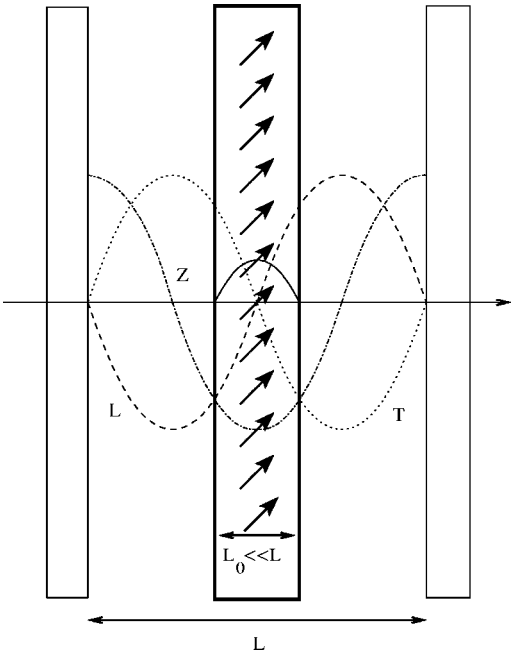

FIG. 2. A molecular crystal slab of width L_0 is located between the cavity mirrors which are separated by distance L. The L, T, and Z components of the $m=2$ cavity modes and the first exciton mode are plotted.

II. THE MICROCAVITY PHOTON

In this section, we consider the microcavity photons. The two infinite and parallel perfect mirrors are in the $(x-y)$ plane, separated by a distance L on the z axis, one mirror is at $z=L/2$, and the other at $z=-L/2$, see Figs. 1 and 2. The electromagnetic field is confined in the z direction, and is free in the cavity plane. The in-plane wave vector is denoted by $\mathbf{q}$, and the z component of the wave vector, q_z, is quantized and has the values $q_z=m\pi/L$, where $(m=1, 2, 3, \ldots)$. The cavity-mode frequencies are given by

$$\omega_{\mathbf{q}m}=\frac{c}{\sqrt{\epsilon}}\sqrt{q^2+\left(\frac{m\pi}{L}\right)^2}, \tag{1}$$

where ϵ is the background dielectric constant of the medium between the mirrors, c is the light velocity, and where $q=|\mathbf{q}|$.

For each in-plane wave vector $\mathbf{q}$ there are two possible polarizations:[13] (TE) modes with transverse electric field, which is denoted by (s), and (TM) modes with transverse magnetic field, which is denoted by (p). The cavity-mode Hamiltonian reads

$$H_{cav}=\sum_{\mathbf{q}m\lambda}\hbar\omega_{\mathbf{q}m}a^{\dagger}_{\mathbf{q}m\lambda}a_{\mathbf{q}m\lambda}, \tag{2}$$

where $a^{\dagger}_{\mathbf{q}m\lambda}$ and $a_{\mathbf{q}m\lambda}$ are the creation and annihilation operators of the $(\mathbf{q}m\lambda)$ photon, respectively, with $(\lambda=s,p)$, and which obey the boson commutation relations. The simple cavity model considered here leads to two degenerate mode polarizations, which is, however, not always the case for more complicated realizations of optical confinement.[14] We will assume only one relevant cavity mode at a time in the z direction, the one which is close to resonance with the organic slab excitons. In fact, from the cavity mode dispersion of Eq. (1), at zero in-plane wave vector $q=0$, the difference between each two adjacent cavity modes is $\Delta E_n=\hbar\omega_{n+1}-\hbar\omega_n=(hc)/(2\sqrt{\epsilon}L)$. Taking $\epsilon=4$ as an average value for the medium filling the cavity and assuming $L=1700$ Å, we get $\Delta E_n\approx 1.8$ eV. As this difference is large enough compared to the typical values of Rabi splitting, Davydov splitting and cavity-exciton detuning considered below, we will include only one relevant cavity mode at a time.

The cavity electric field operator[15] is

$$\hat{\mathbf{E}}(\mathbf{r},z)=-i\sum_{\mathbf{q}m\lambda}\sqrt{\frac{4\pi\hbar\omega_{\mathbf{q}m}}{L\mathcal{A}\epsilon}}\{\mathbf{C}^m_{\lambda}(\mathbf{q},z)e^{i\mathbf{q}\cdot\mathbf{r}}a_{\mathbf{q}m\lambda}-\mathbf{C}^{m*}_{\lambda}(\mathbf{q},z)e^{-i\mathbf{q}\cdot\mathbf{r}}a^{\dagger}_{\mathbf{q}m\lambda}\}, \tag{3}$$

where the location inside the cavity is $(\mathbf{r},z)$, and $\mathcal{A}$ is the in-plane quantization area. The electric field vector functions are

$$\mathbf{C}^m_s(\mathbf{q},z)=\sin\left[\frac{m\pi}{L}\left(z+\frac{L}{2}\right)\right]\hat{\mathbf{n}}_{\mathbf{q}},$$

$$\mathbf{C}^m_p(\mathbf{q},z)=-\left(\frac{cm\pi}{\sqrt{\epsilon}L\omega_{\mathbf{q}m}}\right)\left\{i\sin\left[\frac{m\pi}{L}\left(z+\frac{L}{2}\right)\right]\hat{\mathbf{e}}_{\mathbf{q}}-\frac{|\mathbf{q}|L}{m\pi}\cos\left[\frac{m\pi}{L}\left(z+\frac{L}{2}\right)\right]\hat{\mathbf{e}}_z\right\}, \tag{4}$$

where the unit vectors are: $\hat{\mathbf{n}}_{\mathbf{q}}=\hat{\mathbf{e}}_{\mathbf{q}}\times\mathbf{e}_z$ in the direction perpendicular to $\mathbf{q}$ (transverse component T), and $\hat{\mathbf{e}}_{\mathbf{q}}=\mathbf{q}/|\mathbf{q}|$ in

the direction parallel to **q** (longitudinal component L). The (p) modes include both longitudinal L and Z components, and the (s) modes include the transverse T component only. The cavity mode Z component is of the order of $(qc)/(\sqrt{\epsilon}\omega_{\mathbf{q}m})$, which is small in the spectral region of interest. The cavity modes with ($m=1$) are illustrated in Fig. 1, and those with ($m=2$) in Fig. 2.

III. FRENKEL EXCITONS IN AN ANISOTROPIC ORGANIC CRYSTAL SLAB

The cavity optically resonant material is an anisotropic organic molecular crystal, e.g., an aromatic crystal,[16] which has a proper translational symmetry. In organic crystals the molecules retain their identity, where the wave function overlaps are neglected, and the molecules are bounded by the van der Waals forces. The *Frenkel exciton*, which is an electronic excitation typical of molecular crystals, can transfer between the crystal molecules due to the electrostatic interactions.[17] Such an excitation is described by a wave that propagates in the crystal with wave vector **k**. In this section we calculate the Frenkel exciton dispersion relations in an anisotropic organic slab. We follow the microscopic theory which is applied to derive the Frenkel exciton dispersion relations in organic bulk crystals,[8,12] where we emphasize the distinctions for the case of organic crystal slabs. Other approaches have been applied to study such a system, for instance in Ref. 18 the classical oscillator theory of excitons and polaritons in molecular crystals is used. For each molecule in the crystal we consider the possibility of a single excitation, where the other excited state energies are far from the one considered. We treat the case of very low concentration of excitons. Then, the exciton-exciton interactions can be neglected. In the limit of low exciton concentrations, to a good approximation, the excitons behave as Boson particles.[19]

We assume a thin slab, where the slab width L_0 is much smaller than the distance between the mirrors. Therefore, we can neglect the interactions between the slab excitons and the cavity mirrors. Consequently, the excitons are free in the slab plane, and are confined in the perpendicular direction, and in this direction the exciton wave vector has discrete values. The slab can be divided into N interacting monolayers, where each monolayer includes $M \gg 1$ in-plane unit cells, as appear in Fig. 3. In the following we consider the two cases of anisotropic organic crystals with one and two molecules per unit cell.

A. One molecule per unit cell

The Frenkel exciton Hamiltonian in an organic crystal slab with one molecule per unit cell, by applying the Heitler-London approximation, is given by

$$H_{ex} = \hbar(\omega_0 + D)\sum_{\mathbf{n}} B_{\mathbf{n}}^{\dagger} B_{\mathbf{n}} + \sum_{\mathbf{n},\mathbf{m}} J_{\mathbf{nm}} B_{\mathbf{n}}^{\dagger} B_{\mathbf{m}}, \tag{5}$$

where $B_{\mathbf{n}}^{\dagger}$ and $B_{\mathbf{n}}$ are the creation and annihilation operators of an excitation at site **n**, respectively. The first term describes the excitations of the molecules, where ω_0 is the independent molecule frequency transition, and D is the gas to solid molecule frequency shift due to the interactions of an excited molecule with the other crystal molecules which are at the ground state, where D being usually negative. Note that D for molecules in the outer monolayers of the slab is different from that of the internal ones, as the molecules of the outer monolayers have different neighbor molecules than those of the internal monolayers.[20] Such small differences in D are in the following neglected. The second term in the Hamiltonian describes the excitation transfer between molecules at different sites, where $J_{\mathbf{nm}}$ is the interaction parameter between two molecules at sites **n** and **m**.

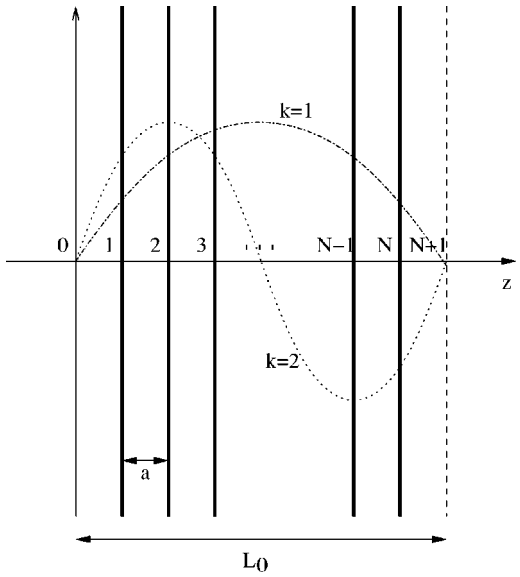

FIG. 3. A slab of N interacting monolayers. The first two exciton modes in the z direction are plotted.

In the slab we assume interactions only between nearest neighbor monolayers. This assumption enables us to treat easily the broken symmetry in the perpendicular direction. The above Hamiltonian can be easily diagonalized by the transformation

$$B_{\mathbf{n}} = \sqrt{\frac{2}{M(N+1)}}\sum_{\mathbf{k},k_z} \sin(k_z z_n) e^{i\mathbf{k}\cdot\mathbf{n}_{\parallel}} B_{\mathbf{k},k_z}, \tag{6}$$

where the site location is defined by $\mathbf{n}=(\mathbf{n}_{\parallel}, z_n)$, with $\mathbf{n}_{\parallel}$ as the location of the site in the monolayer plane, and z_n as the location of the monolayer on the z axis. We assumed $N+2$ monolayers, which are located at $z_n = an$ with $(n=0,1,\ldots,N,N+1)$, and a is the distance between each two neighbor monolayers. As a boundary condition we take the monolayers ($n=0$) and ($n=N+1$) as nodal planes for the exciton wave functions. Here, **k** is the in-plane exciton wave vector, which takes $M \gg 1$ values, as the number of unit cells in each monolayer. k_z is the exciton wave vector in the z direction, is discrete and takes the values $k_z a = \pi l/(N+1)$, with ($l=1,2,\ldots,N$), as the monolayers number in the slab. The first two modes are plotted in Fig. 3.

The diagonal Hamiltonian reads

$$H_{ex} = \sum_{\mathbf{k},k_z} E(\mathbf{k},k_z) B^{\dagger}_{\mathbf{k},k_z} B_{\mathbf{k},k_z}, \tag{7}$$

where the exciton energies are

$$E(\mathbf{k},k_z) = \hbar(\omega_0 + D) + V(\mathbf{k},k_z) \tag{8}$$

with

$$V(\mathbf{k},k_z) = J(\mathbf{k},0) + J(\mathbf{k},k_z). \tag{9}$$

We obtained two exciton dynamical matrices. The exciton dynamical matrix $J(\mathbf{k},0)$, for interactions between molecules in the same monolayer, is defined by

$$J(\mathbf{k},0) = \sum_{\mathbf{L}} J(\mathbf{L},0) e^{i\mathbf{k}\cdot\mathbf{L}}, \tag{10}$$

where we assumed that the interaction parameter is a function of the distance between the molecules, namely $J_{\mathbf{nm}} = J(\mathbf{L})$, with $\mathbf{L} = \mathbf{m}_{\parallel} - \mathbf{n}_{\parallel}$ inside the same monolayer. The exciton dynamical matrix $J(\mathbf{k},k_z)$, for interactions between molecules from two nearest neighbor monolayers, is defined by

$$J(\mathbf{k},k_z) = 2\left\{ \sum_{\mathbf{L}} J(\mathbf{L},a) e^{i\mathbf{k}\cdot\mathbf{L}} \right\} \cos(k_z a). \tag{11}$$

To get the explicit exciton dispersion relation one need to calculate the above dynamical matrices for a crystal with a specific symmetry. Several summation methods for the bulk case have been developed, i.e. in Ref. 21. For illustration, we calculated these matrices for the case of a cubic crystal with lattice constant a, where each molecule has the same transition dipole moment $\vec{\mu} = (\mu_x, \mu_y, \mu_z)$. The cubic axes of the crystal are $\hat{\mathbf{x}}$, $\hat{\mathbf{y}}$, and $\hat{\mathbf{z}}$. The interaction between the crystal molecules is given by the dipole-dipole interaction

$$J(\mathbf{M}) = \frac{|\vec{\mu}|^2 |\mathbf{M}|^2 - 3(\vec{\mu}\cdot\mathbf{M})^2}{|\mathbf{M}|^5}, \tag{12}$$

where we have $\mathbf{M} = (\mathbf{L}, Z) = a(l_x, l_y, l_z)$, with l_x and l_y are the in-plane indexes of each monolayer, and l_z is the perpendicular direction index. The dynamical matrix can be written as

$$V(\mathbf{k},k_z) = \sum_{i,j} V_{i,j}(\mathbf{k},k_z), \tag{13}$$

with

$$V_{i,j}(\mathbf{k},k_z) = \frac{\mu_i \mu_j}{a^3} \{ D_{i,j}(\mathbf{k}, l_z = 0) + 2\cos(k_z a) D_{i,j}(\mathbf{k}, l_z = 1) \}, \tag{14}$$

where

$$D_{i,j}(\mathbf{k},l_z) = \sum_{l_x,l_y}{}' D_{i,j}(l_x,l_y,l_z) e^{ia(k_x l_x + k_y l_y)}, \tag{15}$$

we used $\mathbf{k} = (k_x, k_y)$, with

$$D_{i,j}(l_x,l_y,l_z) = \frac{\delta_{i,j}}{(l_x^2 + l_y^2 + l_z^2)^{3/2}} - 3\frac{l_i l_j}{(l_x^2 + l_y^2 + l_z^2)^{5/2}}, \tag{16}$$

where $(i,j = x,y,z)$. The sum is over all the unit cells in the monolayer, and the prime on the sum indicates that when $l_z = 0$ then the term with $l_x = l_y = 0$ is excluded. Due to the fact that the sum converges very slowly in an oscillatory manner, we should convert this sum into a series which converges very rapidly. To calculate the summation of the exciton dynamical matrix we adopt the procedure that is suggested by Benson and Mills[22] for spin waves in thin films. Philpott[18] used the results of Ref. 22 to derive the exciton and polariton dispersions in molecular mono-layers by using a classical dielectric theory.

In the limit of long waves, that is $ka \ll 1$, where $k = \sqrt{k_x^2 + k_y^2}$, the diagonal dynamical matrix elements are

$$V_{xx}^{\alpha\beta}(\mathbf{k},k_z) = \frac{\mu_x^{\alpha}\mu_x^{\beta}}{a^3}\left\{ 4\pi\cos(k_z a)\frac{k_x^2 a}{k} e^{-ak} - F \right\},$$

$$V_{yy}^{\alpha\beta}(\mathbf{k},k_z) = \frac{\mu_y^{\alpha}\mu_y^{\beta}}{a^3}\left\{ 4\pi\cos(k_z a)\frac{k_y^2 a}{k} e^{-ak} - F \right\},$$

$$V_{zz}^{\alpha\beta}(\mathbf{k},k_z) = \frac{\mu_z^{\alpha}\mu_z^{\beta}}{a^3}\left\{ 2F - \frac{4\pi}{3}\cos(k_z a) ka e^{-ak} \right\}, \tag{17}$$

where

$$F = \tfrac{4}{9}\pi^2 + \tfrac{32}{3}\sum_{n=1}^{\infty}\sum_{l=1}^{\infty} \pi^2 n^2 K_2(2l\pi n), \tag{18}$$

and where $K_2(x)$ is the modified Bessel function of the second order.[23] The off-diagonal dynamical matrix elements are

$$V_{xy}^{\alpha\beta}(\mathbf{k},k_z) = \left(\frac{\mu_x^{\alpha}\mu_y^{\beta}}{a^3}\right) 4\pi\cos(k_z a)\frac{k_x k_y a}{k} e^{-ak},$$

$$V_{xz}^{\alpha\beta}(\mathbf{k},k_z) = -i\left(\frac{\mu_x^{\alpha}\mu_z^{\beta}}{a^3}\right) 4\pi\cos(k_z a) k_x a e^{-ak},$$

$$V_{yz}^{\alpha\beta}(\mathbf{k},k_z) = -i\left(\frac{\mu_y^{\alpha}\mu_z^{\beta}}{a^3}\right) 4\pi\cos(k_z a) k_y a e^{-ak}, \tag{19}$$

with $V_{ji}^{\alpha\beta}(\mathbf{k},k_z) = \{V_{ij}^{\alpha\beta}(\mathbf{k},k_z)\}^*$.

In the present case of one molecule per unit cell the indexes α and β in Eqs. (17) and (19) can be dropped. We added them here for later use in the case of two molecules per unit cell, where they stand for the two orthogonal transition dipole moments defined below. Identical results are obtained by Fuchs and Kliewer[24] for optical phonons in ionic crystals.

The terms that include F in Eqs. (17) stem from the summation of Eq. (10) for interactions between molecules in the same monolayer. The other terms stem from the summation of Eq. (11) for interactions between molecules from two adjacent monolayers. All these terms include the factor $(ka)e^{-ak}$ and lead to a weak anisotropy effect of the order of ka. We note that also the interaction with next nearest monolayers

and more distant ones would be small compared to that within the same monolayer of order F. We obtain that the exciton dispersion relation is an analytical function, where in the limit of $k\to 0$ we get the same result for different directions, which is in contrast to the bulk case where the dispersion exhibits a nonanalytical behavior at small wave vectors.[25]

By summing all the above matrix elements, the exciton dynamical matrix for one molecule per unit cell crystals is given by

$$V(\mathbf{k},k_z)=\frac{4\pi}{3a^3}\cos(k_z a)e^{-ak}(ka)\{3(\vec{\mu}_\parallel\cdot\hat{k})^2-\mu_z^2\}+\frac{F}{a^3}\{2\mu_z^2-\mu_\parallel^2\},\tag{20}$$

where the in-plane transition dipole moment is $\vec{\mu}_\parallel=(\mu_x,\mu_y)$, and $\hat{k}=\mathbf{k}/k$. From Eq. (20) we see that the two-dimensional exciton dispersion, at small values of k, shows for the L and Z modes a linear dependence on k, which is due to the long range contribution of the Coulomb interaction (as also discussed in Refs. 18 and 26). For zero in-plane wave vector, $k=0$, we have $V(0)=(F/a^3)\{2\mu_z^2-\mu_\parallel^2\}$. For the case of $\mu_z=0$ we get $V(0)=-(F/a^3)\mu_\parallel^2$, and for the case of $\mu_\parallel=0$ we have $V(0)=(2F/a^3)\mu_z^2$. This difference between the exciton dynamical matrix for the z and the in-plane dipole moment cases, at $k=0$, is a polarization splitting (also known as depolarization shift), and was obtained also in inorganic semiconductor thin layers.[18,26]

B. Two molecules per unit cell

In this section we consider an anisotropic molecular crystal slab with two molecules per unit cell, where the two molecules are chemically identical, but they have different orientations. The Frenkel exciton Hamiltonian, in the Heitler-London approximation, is

$$H=\hbar(\omega_0+D)\sum_{\mathbf{n},i}B_{\mathbf{n}i}^\dagger B_{\mathbf{n}i}+\sum_{\mathbf{nm},ij}J^{ij}(\mathbf{n}-\mathbf{m})B_{\mathbf{n}i}^\dagger B_{\mathbf{m}j},\tag{21}$$

where $(i,j=1,2)$, for the two kinds of molecules in each unit cell. Here, the interaction parameter $J^{ij}(\mathbf{n}-\mathbf{m})$, which is a function of the distance between the two molecules, includes interactions between two different sites, which are $J^{11}(\mathbf{n}-\mathbf{m})$, $J^{22}(\mathbf{n}-\mathbf{m})$, $J^{21}(\mathbf{n}-\mathbf{m})$ and $J^{12}(\mathbf{n}-\mathbf{m})$; and includes interactions between the two different molecules in the same site, which are $J_{12}=J_{21}$. We assume that the molecules have the transition dipole moments $\vec{\mu}_1$ and $\vec{\mu}_2$, where $|\vec{\mu}_1|=|\vec{\mu}_2|$. We define the two orthogonal transition dipole moments

$$\vec{\mu}_+=\frac{\vec{\mu}_1+\vec{\mu}_2}{\sqrt{2}},\quad \vec{\mu}_-=\frac{\vec{\mu}_1-\vec{\mu}_2}{\sqrt{2}},\quad \vec{\mu}_+\perp\vec{\mu}_-.\tag{22}$$

In the following we calculate the exciton dispersion relations. We will deal separately with the two cases: (i) in-plane dipole moments and (ii) general dipole moments which include z components. Due to the broken symmetry in the z direction, we will get different dispersion relations for the two cases.

1. In-plane molecule dipole moments

To diagonalize the above exciton Hamiltonian, as before, the slab is divided into N interacting monolayers, where each monolayer includes $M\gg 1$ unit cells. We assume interactions only between the nearest neighbor monolayers. The diagonal Hamiltonian reads

$$H=\sum_{\mathbf{k}k_z,\nu}E_\nu(\mathbf{k},k_z)B_{\mathbf{k}k_z}^{\nu\dagger}B_{\mathbf{k}k_z}^{\nu},\tag{23}$$

where we obtained two exciton branches which are denoted by $(\nu=a,b)$. To diagonalize the Hamiltonian, the following transformation is used:

$$B_{\mathbf{n}1}=\sqrt{\frac{1}{M(N+1)}}\sum_{\mathbf{k}k_z}\sin(k_z z_n)e^{i\mathbf{k}\cdot\mathbf{n}_\parallel}\{B_{\mathbf{k}k_z}^a+B_{\mathbf{k}k_z}^b\},$$

$$B_{\mathbf{n}2}=\sqrt{\frac{1}{M(N+1)}}\sum_{\mathbf{k}k_z}\sin(k_z z_n)e^{i\mathbf{k}\cdot\mathbf{n}_\parallel}\{B_{\mathbf{k}k_z}^a-B_{\mathbf{k}k_z}^b\}.\tag{24}$$

The two exciton dispersion branches, corresponding to the two orthogonal dipole moments, are

$$E_a(\mathbf{k},k_z)=\hbar(\omega_0+D)+J_{12}+V^{++}(\mathbf{k},k_z),$$

$$E_b(\mathbf{k},k_z)=\hbar(\omega_0+D)-J_{12}+V^{--}(\mathbf{k},k_z),\tag{25}$$

where $V^{\alpha\beta}(\mathbf{k},k_z)=J^{\alpha\beta}(\mathbf{k},0)+J^{\alpha\beta}(\mathbf{k},k_z)$, with the exciton dynamical matrices

$$J^{\alpha\beta}(\mathbf{k},0)=\sum_{\mathbf{L}}{}'J^{\alpha\beta}(\mathbf{L},0)e^{i\mathbf{k}\cdot\mathbf{L}},$$

$$J^{\alpha\beta}(\mathbf{k},k_z)=2\left\{\sum_{\mathbf{L}}{}'J^{\alpha\beta}(\mathbf{L},a)e^{i\mathbf{k}\cdot\mathbf{L}}\right\}\cos(k_z a).\tag{26}$$

The first term represents the sum over interactions between molecules in the same monolayer, and the second represents interactions between molecules from two nearest neighbor monolayers. The prime indicates that the interactions between molecules from the same unit cell are excluded. The interactions in the same unit cell, J_{12}, are included explicitly in the above diagonal energies Eqs. (25). The dynamical matrix elements for the case of a crystal with cubic symmetry are given in Eqs. (17)–(19). The exciton band splits into the two branches (a) and (b) which are separated by the Davydov splitting energy, which is

$$\Delta_D=2J_{12}+V^{++}(\mathbf{k},k_z)-V^{--}(\mathbf{k},k_z).\tag{27}$$

This splitting is due to the existence of two molecules per unit cell. The $B_{\mathbf{k},k_z}^a$ and $B_{\mathbf{k},k_z}^b$ excitons include, respectively, only the $\vec{\mu}_+$ and $\vec{\mu}_-$ orthogonal dipoles.

Now, we will examine the exciton dynamical matrix in detail. The relations between the exciton dynamical matrix elements in terms of the orthogonal dipole moments and that in terms of the original dipole moments, are given by

$$V^{++}(\mathbf{k},k_z)=\left[\frac{V^{11}(\mathbf{k},k_z)+V^{22}(\mathbf{k},k_z)+V^{21}(\mathbf{k},k_z)+V^{12}(\mathbf{k},k_z)}{2}\right],$$

$$V^{--}(\mathbf{k},k_z)=\left[\frac{V^{11}(\mathbf{k},k_z)+V^{22}(\mathbf{k},k_z)-V^{21}(\mathbf{k},k_z)-V^{12}(\mathbf{k},k_z)}{2}\right],$$

$$V^{+-}(\mathbf{k},k_z)=\left[\frac{V^{11}(\mathbf{k},k_z)-V^{22}(\mathbf{k},k_z)+V^{21}(\mathbf{k},k_z)-V^{12}(\mathbf{k},k_z)}{2}\right]. \tag{28}$$

In the case of bulk crystal with inversion symmetry,[12] we get

$$V^{11}(\mathbf{k},k_z)=V^{22}(\mathbf{k},k_z),\quad V^{12}(\mathbf{k},k_z)=V^{21}(\mathbf{k},k_z), \tag{29}$$

that is the exciton dynamical matrix is real and symmetric. Hence, we get $V^{+-}(\mathbf{k},k_z)=0$. These results still hold here also in our system of an organic crystal slab in the case of in-plane dipole moments, where $\vec{\mu}_\nu\cdot\hat{\mathbf{z}}=0$. It is seen from the results of Eqs. (17) and (19), for the case of cubic crystals, that in the case of in-plane dipole moments, the dynamical matrix is real and symmetric, where we retain the inversion symmetry in the slab plane. This fact leads to the exciton energies of Eqs. (25). In comparison with the results of organic crystal bulks with inversion symmetry,[12] the differences stem from the exciton confinement in the perpendicular direction and from the assumption of interaction between nearest neighbor monolayers only.

2. General molecule dipole moments

In the case of general dipole moments with *z* components, where $\vec{\mu}_\nu\cdot\hat{\mathbf{z}}\neq 0$, the results of Eqs. (29) are not satisfied in general, and we have $V^{+-}(\mathbf{k},k_z)\neq 0$. We show that this leads to different dispersion relations for the exciton branches. In the following we obtain that each Davydov exciton branch is related to both the orthogonal dipole moments, $\vec{\mu}_\pm$. The diagonal Hamiltonian is still given by Eq. (23), but with the diagonal energies

$$E_a(\mathbf{k},k_z)=\left(\frac{A_+(\mathbf{k},k_z)+A_-(\mathbf{k},k_z)}{2}\right)+\Delta(\mathbf{k},k_z),$$

$$E_b(\mathbf{k},k_z)=\left(\frac{A_+(\mathbf{k},k_z)+A_-(\mathbf{k},k_z)}{2}\right)-\Delta(\mathbf{k},k_z), \tag{30}$$

where

$$A_+(\mathbf{k},k_z)=E_++V^{++}(\mathbf{k},k_z),$$

$$A_-(\mathbf{k},k_z)=E_-+V^{--}(\mathbf{k},k_z), \tag{31}$$

and where

$$\Delta^2(\mathbf{k},k_z)=\mathcal{S}^2(\mathbf{k},k_z)+|V^{+-}(\mathbf{k},k_z)|^2,$$

$$\mathcal{S}(\mathbf{k},k_z)=\frac{A_+(\mathbf{k},k_z)-A_-(\mathbf{k},k_z)}{2}, \tag{32}$$

and with $E_\pm=\hbar(\omega_0+D)\pm J_{12}$. The exciton dynamical matrix is $V^{\alpha\beta}(\mathbf{k},k_z)=J^{\alpha\beta}(\mathbf{k},0)+J^{\alpha\beta}(\mathbf{k},k_z)$, where $J^{\alpha\beta}(\mathbf{k},0)$ and $J^{\alpha\beta}(\mathbf{k},k_z)$ are defined in Eqs. (26), and their matrix element summations, for long wave lengths and in cubic crystals, are given in Eqs. (17)–(19). We obtain two exciton branches, *a* and *b*, which are separated by the Davydov energy splitting $E_a(\mathbf{k},k_z)-E_b(\mathbf{k},k_z)=2\Delta(\mathbf{k},k_z)$. By substituting $V^{+-}(\mathbf{k},k_z)=0$, the results of the previous section for the case of in-plane dipole moments are recovered. The general transformation, which is used in order to diagonalize the whole Hamiltonian, is given by

$$B_{\mathbf{n}1}=\frac{1}{\sqrt{M(N+1)}}\sum_{\mathbf{k}k_z}\sin(k_zz_r)e^{i\mathbf{k}\cdot\mathbf{n}_\parallel}\times\sum_{\nu=ab}[R^+_\nu(\mathbf{k},k_z)+R^-_\nu(\mathbf{k},k_z)]B^\nu_{\mathbf{k}k_z},$$

$$B_{\mathbf{n}2}=\frac{1}{\sqrt{M(N+1)}}\sum_{\mathbf{k}k_z}\sin(k_zz_r)e^{i\mathbf{k}\cdot\mathbf{n}_\parallel}\times\sum_{\nu=ab}[R^+_\nu(\mathbf{k},k_z)-R^-_\nu(\mathbf{k},k_z)]B^\nu_{\mathbf{k}k_z}, \tag{33}$$

where

$$R^+_a(\mathbf{k},k_z)=\sqrt{\frac{\Delta(\mathbf{k},k_z)+\mathcal{S}(\mathbf{k},k_z)}{2\Delta(\mathbf{k},k_z)}},$$

$$R^-_a(\mathbf{k},k_z)=\frac{V^{-+}(\mathbf{k},k_z)}{\sqrt{2\Delta(\mathbf{k},k_z)[\Delta(\mathbf{k},k_z)+\mathcal{S}(\mathbf{k},k_z)]}},$$

$$R^+_b(\mathbf{k},k_z)=-\sqrt{\frac{\Delta(\mathbf{k},k_z)-\mathcal{S}(\mathbf{k},k_z)}{2\Delta(\mathbf{k},k_z)}},$$

$$R^-_b(\mathbf{k},k_z)=\frac{V^{-+}(\mathbf{k},k_z)}{\sqrt{2\Delta(\mathbf{k},k_z)[\Delta(\mathbf{k},k_z)-\mathcal{S}(\mathbf{k},k_z)]}}. \tag{34}$$

Due to the *z* direction broken symmetry, and in the existence of the dipole moment *z* components, each one of the Davydov exciton branches, *a* and *b*, includes both the orthogonal dipole moments, (+) and (−). This fact is clear from the existence of a nonvanishing $V^{+-}(\mathbf{k},k_z)$ dynamical matrix. In the limit of $V^{+-}(\mathbf{k},k_z)\to 0$ we get R^+_a, $R^-_b\to 1$ and R^-_a, $R^+_b\to 0$, recovering the results of Eqs. (24) for the case of in-plane dipole moments.

IV. ANISOTROPIC ORGANIC CAVITY EXCITON POLARITONS

The excitons in the organic slab and the cavity modes are coherently coupled to produce the cavity exciton polaritons. The anisotropic organic slab of width $L_0\ll L$ is located in the middle between the cavity mirrors, at $z\sim 0$, and is parallel to the cavity mirrors, see Figs. 1 and 2. For the excitons we assume only one dominant mode in the *z* direction, the lowest energy mode which has no nodes, with the *z* component wave vector $k_za=\pi/(N+1)$. For the coupling between the excitons and the cavity modes we use the dipole approximation. The coupling Hamiltonian is $V=-\hat{\mu}\cdot\hat{\mathbf{E}}$, where $\hat{\mu}$ is the

organic slab dipole moment operator, and $\hat{\mathbf{E}}$ is the cavity electric field operator. Due to the thin slab approximation, that is $q_z L_0 \ll 1$, where q_z is the z component of the cavity photon wave vector, the electric field is evaluated at $z=0$. Furthermore, we will apply the rotating wave approximation in deriving the coupling Hamiltonian. In the cavity we assume only one relevant cavity mode in the z direction at a time, the $(m=1)$ or the $(m=2)$ one. In the following we investigate the two cases of organic cavities with one and two molecules per unit cell.

A. One molecule per unit cell

For the case of an organic crystal slab with one molecule per unit cell, the dipole moment operator of the molecule at site $\mathbf{n}$ is $\hat{\mu}_{\mathbf{n}}=\vec{\mu}B_{\mathbf{n}}^{\dagger}+\vec{\mu}^{*}B_{\mathbf{n}}$. The transition exciton dipole moment is in general coupled with both cavity-mode polarizations, (s) and (p). This fact is in contrast to the case of usual inorganic semiconductor crystals,[26] where the (s) modes interact with the T exciton components, and the (p) modes interact with the L and Z exciton components. The coupled exciton and cavity-mode Hamiltonian reads

$$H=\sum_{\mathbf{k}}\left\{\hbar\omega_{\mathbf{k}}^{ex}B_{\mathbf{k}}^{\dagger}B_{\mathbf{k}}+\sum_{\lambda=s,p}\hbar\omega_{\mathbf{k}}^{cav}a_{\mathbf{k}\lambda}^{\dagger}a_{\mathbf{k}\lambda}+\sum_{\lambda=s,p}\hbar[f_{\mathbf{k}\lambda}B_{\mathbf{k}}^{\dagger}a_{\mathbf{k}\lambda}+f_{\mathbf{k}\lambda}^{*}a_{\mathbf{k}\lambda}^{\dagger}B_{\mathbf{k}}]\right\}. \quad (35)$$

The coupling is between excitons and cavity-modes of both polarization with the same in-plane wave vector, as dictated by in-plane translational symmetry. The coupling parameter is given by

$$f_{\mathbf{k}\lambda}=i\sqrt{\frac{8\pi M\hbar\omega_{\mathbf{k}}^{cav}}{L\mathcal{A}\epsilon(N+1)}}[\vec{\mu}\cdot\mathbf{C}_{\lambda}(\mathbf{k})]\cot\left[\frac{\pi}{2(N+1)}\right], \quad (36)$$

where $\mathbf{C}_{\lambda}(\mathbf{k})$ is defined by Eqs. (4) evaluated at $z=0$, and where $\cot(x)=1/\tan(x)$.

The diagonalization of the above Hamiltonian gives the polariton Hamiltonian

$$H_{pol}=\sum_{\mathbf{k}r}\hbar\Omega_{r}(\mathbf{k})A_{\mathbf{k}}^{r\dagger}A_{\mathbf{k}}^{r}, \quad (37)$$

with the polariton dispersion relations

$$\Omega_{\pm}(\mathbf{k})=\frac{\omega_{\mathbf{k}}^{ex}+\omega_{\mathbf{k}}^{cav}}{2}\pm\Delta_{\mathbf{k}},\quad \Omega_{0}(\mathbf{k})=\omega_{\mathbf{k}}^{cav}, \quad (38)$$

where we obtain three polariton branches. The upper, $(+)$, and the lower, $(-)$, branches are separated by the Rabi splitting energy, $2\Delta_{\mathbf{k}}$, where $\Delta_{\mathbf{k}}^{2}=\delta_{\mathbf{k}}^{2}+f_{\mathbf{k}}^{2}$. We define the exciton and cavity-mode detuning $\delta_{\mathbf{k}}=(\omega_{\mathbf{k}}^{ex}-\omega_{\mathbf{k}}^{cav})/2$, and the general exciton and cavity-mode coupling parameter $f_{\mathbf{k}}^{2}=\Sigma_{\lambda}|f_{\mathbf{k}\lambda}|^{2}$. The polariton operators are defined by

$$A_{\mathbf{k}}^{\pm}=C_{\mathbf{k}}^{\pm}B_{\mathbf{k}}+\sum_{\lambda}X_{\mathbf{k}\lambda}^{\pm}a_{\mathbf{k}\lambda},\quad A_{\mathbf{k}}^{0}=\sum_{\lambda}X_{\mathbf{k}\lambda}^{0}a_{\mathbf{k}\lambda}, \quad (39)$$

where

$$C_{\mathbf{k}}^{\pm}=\pm\sqrt{\frac{\Delta_{\mathbf{k}}\pm\delta_{\mathbf{k}}}{2\Delta_{\mathbf{k}}}},\quad X_{\mathbf{k}\lambda}^{\pm}=\frac{f_{\mathbf{k}\lambda}}{\sqrt{2\Delta_{\mathbf{k}}(\Delta_{\mathbf{k}}\pm\delta_{\mathbf{k}})}},$$

$$X_{\mathbf{k}s}^{0}=\frac{f_{\mathbf{k}p}^{*}}{f_{\mathbf{k}}},\quad X_{\mathbf{k}p}^{0}=-\frac{f_{\mathbf{k}s}^{*}}{f_{\mathbf{k}}}. \quad (40)$$

The upper and the lower branches mix the excitons and the two cavity-mode polarizations, while the middle, (0), polariton branch includes only the two cavity-mode polarizations. Due to the existence of a polarization direction where the excitons and the cavity modes are decoupled, we get a pure photonic branch. The inverse operator transformation is given by

$$B_{\mathbf{k}}=\sum_{r}C_{\mathbf{k}}^{r*}A_{\mathbf{k}}^{r},\quad a_{\mathbf{k}\lambda}=\sum_{r}X_{\mathbf{k}\lambda}^{r*}A_{\mathbf{k}}^{r}. \quad (41)$$

Now, we going to study the two cases of cavity modes with $(m=1)$, and $(m=2)$.

1. $(m=1)$ cavity modes

The active mode in the z direction is chosen to be the first one with $(m=1)$, which is illustrated in Fig. 1, then the coupling parameters, by using Eqs. (4) and (36), are given by

$$f_{\mathbf{k}s}=iS(\mathbf{k})(\vec{\mu}\cdot\hat{\mathbf{n}}_{\mathbf{k}}),\quad f_{\mathbf{k}p}=S(\mathbf{k})\sqrt{1-\frac{k^{2}}{Q^{2}}}(\vec{\mu}\cdot\hat{\mathbf{e}}_{\mathbf{k}}), \quad (42)$$

where

$$S(\mathbf{k})=\sqrt{\frac{8\pi M\hbar\omega_{\mathbf{k}}^{cav}}{L\mathcal{A}\epsilon(N+1)}}\cot\left[\frac{\pi}{2(N+1)}\right], \quad (43)$$

with $\mathcal{A}/M=a^{2}$ for cubic crystals. Here

$$Q=\sqrt{k^{2}+\left(\frac{\pi}{L}\right)^{2}}, \quad (44)$$

and $\omega_{\mathbf{k}}^{cav}$ is given in Eq. (1) with $(m=1)$. The Z polarized cavity mode is not coupled with the slab excitons. The molecule dipole moment is $\vec{\mu}=(\mu_x,\mu_y,\mu_z)$. The unit vectors can be written as

$$\hat{\mathbf{e}}_{\mathbf{k}}=\cos\phi\hat{\mathbf{x}}+\sin\phi\hat{\mathbf{y}},\quad \hat{\mathbf{n}}_{\mathbf{k}}=-\sin\phi\hat{\mathbf{x}}+\cos\phi\hat{\mathbf{y}}, \quad (45)$$

where ϕ is the angle between the in-plane wave vector $\mathbf{k}$ and the $\hat{\mathbf{x}}$ axis. If the molecule dipole moment is $\vec{\mu}=(\mu_x,0,\mu_z)$, then the coupling parameters read

$$f_{\mathbf{k}s}=iW(\mathbf{k})\sin\phi,\quad f_{\mathbf{k}p}=W(\mathbf{k})\sqrt{1-\frac{k^{2}}{Q^{2}}}\cos\phi, \quad (46)$$

where $W(\mathbf{k})=S(\mathbf{k})\mu_x$. The upper and lower polariton branch dispersion relations are

$$\Omega_{\pm}(\mathbf{k})=\frac{\omega_{\mathbf{k}}^{ex}+\omega_{\mathbf{k}}^{cav}}{2}\pm\sqrt{\left(\frac{\omega_{\mathbf{k}}^{ex}-\omega_{\mathbf{k}}^{cav}}{2}\right)^{2}+W^{2}(\mathbf{k})\left(1-\frac{k^{2}}{Q^{2}}\cos^{2}\phi\right)}. \quad (47)$$

The anisotropy effect in the polariton dispersions is from the order of k^{2}/Q^{2}. In the limit of long waves, that is $Q\gg k$, the anisotropy effect is negligible and the dispersion relations are

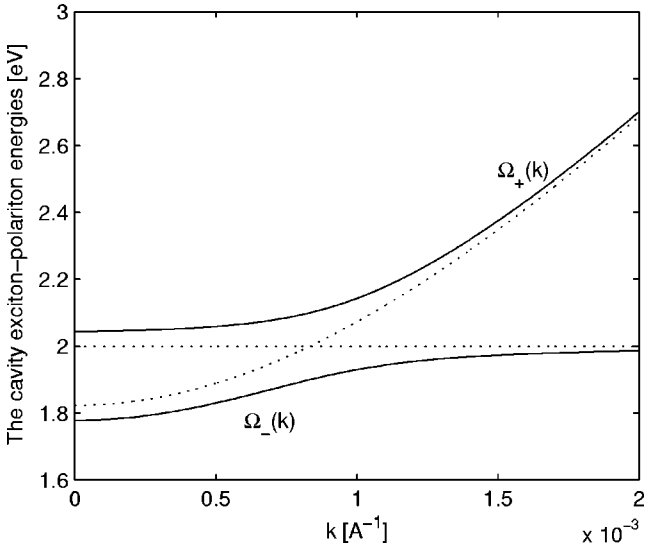

FIG. 4. The two cavity exciton-polariton energies vs in-plane wave vector k. The horizontal dotted line is the exciton dispersion, and the parabolic dotted line is the cavity-mode dispersion.

similar to that of isotropic materials. In this case, identical results were obtained in Ref. 9 by using a macroscopic theory. In Fig. 4 the cavity exciton polaritons are plotted as a function of the in-plane wave vector, k, in the limit of small in-plane wave vector. The exciton and the cavity-mode dispersions mix and split to produce the two polariton branches. For large wave vectors the upper branch coincides with the cavity-mode dispersion, and the lower branch coincides with the exciton one. The Rabi splitting appears at the exciton-cavity mode intersection point. We used typical parameters for organics: the exciton energy, in the limit of small wave vector, is $\hbar\omega^{ex}=2$ eV, the dielectric constant is $\epsilon=4$, and the distance between the cavity mirrors is $L=1700$ Å. In the case of $N=10$ and for lattice constant of $a=15$ Å, we get $S\approx 0.01\sqrt{\text{eV/Å}^3}$, and then the exciton-cavity mode coupling parameter is $\hbar W=0.1$ eV, for dipole moment of $\mu_x=10\sqrt{\text{eV Å}^3}$.

2. (m=2) cavity modes

Now, the active mode in the z direction is chosen to be the second one with $(m=2)$, which is illustrated in Fig. 2, then the coupling parameters, by using Eqs. (4) and (36), are given by

$$f_{\mathbf{k}s}=0, \quad f_{\mathbf{k}p}=-iS(\mathbf{k})\frac{k}{Q}(\vec{\mu}\cdot\hat{\mathbf{e}}_z), \tag{48}$$

where here $Q=\sqrt{k^2+(2\pi/L)^2}$, and $S(\mathbf{k})$ is as defined in Eq. (43). It is seen that only the Z polarized $(m=2)$ cavity mode is coupled with the exciton slab. From Eqs. (4), it is seen that the cavity mode Z component yields coupling parameter from the order of k/Q. The upper and lower polariton branch dispersion relations are

$$\Omega_{\pm}(\mathbf{k})=\frac{\omega_{\mathbf{k}}^{ex}+\omega_{\mathbf{k}}^{cav}}{2}\pm\sqrt{\left(\frac{\omega_{\mathbf{k}}^{ex}-\omega_{\mathbf{k}}^{cav}}{2}\right)^2+S^2(\mathbf{k})\mu_z^2\frac{k^2}{Q^2}}, \tag{49}$$

where $\omega_{\mathbf{k}}^{cav}$ is given in Eq. (1) with $(m=2)$. In the limit of long waves, that is $Q\gg k$, the excitons and cavity-modes coupling is very weak, and the Rabi splitting disappears.

B. Two molecules per unit cell

Each unit cell in the organic crystal slab contains two molecules, the molecules are chemically identical and have different orientations, where the dipole moments are $\vec{\mu}_1$ and $\vec{\mu}_2$. The exciton band splits into two branches, (a) and (b), which are separated by the Davydov splitting energy. Each exciton branch is coupled with the two cavity-mode polarizations, (s) and (p). The total Hamiltonian, of the coupled exciton branches and cavity modes, is given by

$$H=\sum_{\mathbf{k}}\left\{\sum_{\nu}\hbar\omega_{\nu}^{ex}(\mathbf{k})B_{\mathbf{k}}^{\nu\dagger}B_{\mathbf{k}}^{\nu}+\sum_{\lambda}\hbar\omega_{\mathbf{k}}^{cav}a_{\mathbf{k}\lambda}^{\dagger}a_{\mathbf{k}\lambda}+\sum_{\lambda\nu}\hbar(f_{\mathbf{k}\lambda}^{\nu}B_{\mathbf{k}}^{\nu\dagger}a_{\mathbf{k}\lambda}+f_{\mathbf{k}\lambda}^{\nu*}a_{\mathbf{k}\lambda}^{\dagger}B_{\mathbf{k}}^{\nu})\right\}. \tag{50}$$

The coupling is between excitons and cavity-modes with the same in-plane wave vector. We assumed, as before, only one active cavity-mode in the z direction. In this section we consider only cavity-modes with $(m=1)$. For the excitons we assume only one dominant quantized mode in the z direction, which is the first one. To get the polariton dispersion relations we diagonalize the above Hamiltonian. The diagonal Hamiltonian is as given in Eq. (37). From the coupling between the two exciton branches and the two cavity-mode polarizations we obtain four polariton branches. The polariton dispersion relations are the solutions of the relation

$$\begin{aligned}&\{[\Omega_r(\mathbf{k})-\omega_a^{ex}(\mathbf{k})][\Omega_r(\mathbf{k})-\omega_{\mathbf{k}}^{cav}]-(|f_{\mathbf{k}s}^a|^2+|f_{\mathbf{k}p}^a|^2)\}\\&\quad\times\{[\Omega_r(\mathbf{k})-\omega_b^{ex}(\mathbf{k})][\Omega_r(\mathbf{k})-\omega_{\mathbf{k}}^{cav}]-(|f_{\mathbf{k}s}^b|^2+|f_{\mathbf{k}p}^b|^2)\}\\&\quad=|(f_{\mathbf{k}s}^{a*}f_{\mathbf{k}s}^b+f_{\mathbf{k}p}^{a*}f_{\mathbf{k}p}^b)|^2.\end{aligned} \tag{51}$$

In the following we will treat separately the two cases of in-plane dipole moments, and general dipole moments with z components.

1. In-plane molecule dipole moments

Here, we consider the case where the molecule dipole moments are in the slab plane, that is the z components are zero. We use the results of Sec. III B 1. The coupling parameters are

$$f_{\mathbf{k}\lambda}^a=iS(\mathbf{k})[\vec{\mu}_+\cdot\mathbf{C}_\lambda(\mathbf{k})], \quad f_{\mathbf{k}\lambda}^b=iS(\mathbf{k})[\vec{\mu}_-\cdot\mathbf{C}_\lambda(\mathbf{k})], \tag{52}$$

where $S(\mathbf{k})$ is defined in Eq. (43). The coupling parameters are given in terms of the orthogonal dipole moments which are defined in Eqs. (22). The electromagnetic field vector functions are evaluated at $z=0$. At this point we assume that the dipole moment $\vec{\mu}_+$ is in the $\hat{\mathbf{x}}$ direction, and the dipole

moment $\vec{\mu}_-$ is in the $\hat{\mathbf{y}}$ direction, and ϕ is as defined before. The coupling parameters are given by

$$f^b_{\mathbf{k}s} = -iS(\mathbf{k})\mu_- \cos\phi, \quad f^b_{\mathbf{k}p} = S(\mathbf{k})\sqrt{1-\frac{k^2}{Q^2}}\mu_- \sin\phi,$$

$$f^a_{\mathbf{k}s} = iS(\mathbf{k})\mu_+ \sin\phi, \quad f^a_{\mathbf{k}p} = S(\mathbf{k})\sqrt{1-\frac{k^2}{Q^2}}\mu_+ \cos\phi, \tag{53}$$

with Q of Eq. (44). The dispersion relation of Eq. (51) is reduced to

$$\left\{[\Omega_r(\mathbf{k})-\omega^{ex}_a(\mathbf{k})][\Omega_r(\mathbf{k})-\omega^{cav}_{\mathbf{k}}]-W^2_a(\mathbf{k})\left(1-\frac{k^2}{Q^2}\cos^2\phi\right)\right\}$$
$$\times\left\{[\Omega_r(\mathbf{k})-\omega^{ex}_b(\mathbf{k})][\Omega_r(\mathbf{k})-\omega^{cav}_{\mathbf{k}}]\right.$$
$$\left.-W^2_b(\mathbf{k})\left(1-\frac{k^2}{Q^2}\sin^2\phi\right)\right\}$$
$$=W^2_a(\mathbf{k})W^2_b(\mathbf{k})\left(\frac{k^4}{Q^4}\right)\sin^2\phi\cos^2\phi, \tag{54}$$

where $W^2_a(\mathbf{k})=S^2(\mathbf{k})|\mu_+|^2$, and $W^2_b(\mathbf{k})=S^2(\mathbf{k})|\mu_-|^2$. The right hand side is from the order of k^4/Q^4, and is responsible for the mixing between the two exciton Davydov branches. In the limit of small in-plane wave vectors, where $k \ll Q$, we can ignore the right hand side of the above relation. The solution of this equation gives the four polariton frequencies, which are

$$\Omega_{1,2}(\mathbf{k}) = \frac{\omega^{ex}_a(\mathbf{k})+\omega^{cav}_{\mathbf{k}}}{2} \pm \sqrt{\left[\frac{\omega^{ex}_a(\mathbf{k})-\omega^{cav}_{\mathbf{k}}}{2}\right]^2 + W^2_a(\mathbf{k})\left(1-\frac{k^2}{Q^2}\cos^2\phi\right)},$$

$$\Omega_{3,4}(\mathbf{k}) = \frac{\omega^{ex}_b(\mathbf{k})+\omega^{cav}_{\mathbf{k}}}{2} \pm \sqrt{\left[\frac{\omega^{ex}_b(\mathbf{k})-\omega^{cav}_{\mathbf{k}}}{2}\right]^2 + W^2_b(\mathbf{k})\left(1-\frac{k^2}{Q^2}\sin^2\phi\right)}. \tag{55}$$

The anisotropy effect is from the order of k^2/Q^2, which is very weak. The macroscopic theory of Ref. 9 gave identical results for the present case. In the limit of long waves it is seen that the coupling of the excitons and the cavity modes does not mix the two Davydov exciton branches.

In Figs. 5–8 the cavity exciton polaritons are plotted as a function of the in-plane wave vector, k, in the limit of small in-plane wave vector. The four polariton branches appear in the figures, two upper and two lower branches. For large wave vectors the two upper branches coincide with the cavity-mode dispersion, and the lower branches coincide with the two Davydov exciton dispersions. We use typical numbers for organics: the two exciton branch energies at small wave vectors are $\hbar\omega^{ex}_{a,b}=\hbar\omega^{ex}_0\pm\Delta_D$, with $\hbar\omega^{ex}_0=2$ eV, the dielectric constant is $\epsilon=4$, and the distance between the cavity mirrors is $L=1700$ Å. In Fig. 5 the energies are plotted in the case of $W_a\sim W_b\sim\Delta_D$, with a Davydov splitting of $\Delta_D=0.1$ eV. In Fig. 6 the energies are plotted in the case of $W_a\sim W_b\gg\Delta_D$, with a Davydov splitting of $\Delta_D=0.03$ eV. Due to the smallness of the Davydov splitting, the two upper branches are close from each other, and the two lower branches too, whereas we have large Rabi splitting between the upper and lower branches. Figure 7 is for the case of

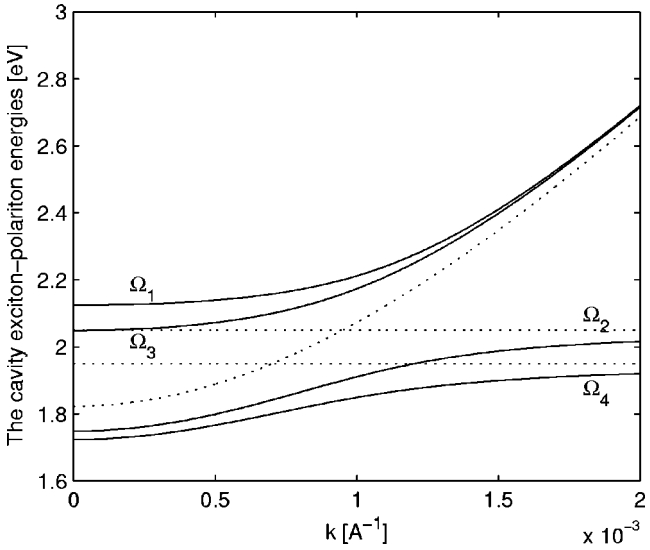

FIG. 5. The four cavity exciton-polariton energies vs in-plane wave vector k, for in-plane dipole moments, in the case of $W_a\sim W_b\sim\Delta_D$, where $\Delta_D=0.1$ eV and $W_a=W_b=0.15$ eV. The horizontal dotted lines are the two Davydov exciton branches, and the parabolic dotted line is the cavity-mode dispersion.

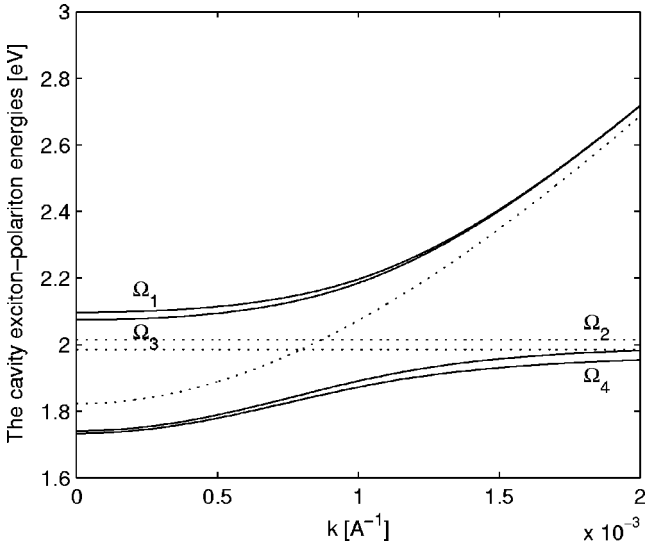

FIG. 6. The four cavity exciton-polariton energies vs in-plane wave vector k, for in-plane dipole moments, in the case of $W_a\sim W_b\gg\Delta_D$, where $\Delta_D=0.03$ eV and $W_a=W_b=0.15$ eV. The horizontal dotted lines are the two Davydov exciton branches, and the parabolic dotted line is the cavity-mode dispersion.

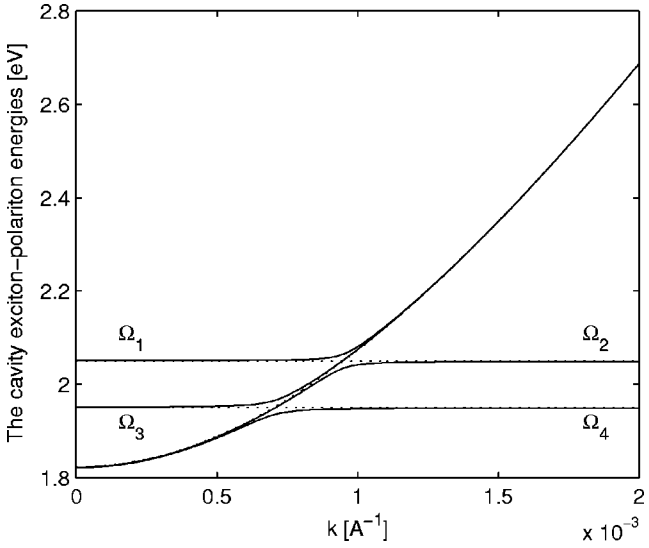

FIG. 7. The four cavity exciton-polariton energies vs in-plane wave vector k, for in-plane dipole moments, in the case of $W_a \sim W_b \ll \Delta_D$, where $\Delta_D = 0.1$ eV and $W_a = W_b = 0.015$ eV. The horizontal dotted lines are the two Davydov exciton branches, and the parabolic dotted line is the cavity-mode dispersion.

$W_a, W_b \ll \Delta_D$, with a Davydov splitting of $\Delta_D = 0.1$ eV. Figure 8 is for the case of $W_a \gg W_b \sim \Delta_D$, where polaritons including the upper Davydov exciton branch have large Rabi splitting, but those including the lower Davydov branch have not.

The polariton operators are defined by the canonical transformation

$$A_{\mathbf{k}}^{r} = \sum_{\nu} C_{\mathbf{k}\nu}^{r} B_{\mathbf{k}}^{\nu} + \sum_{\lambda} X_{\mathbf{k}\lambda}^{r} a_{\mathbf{k}\lambda}, \tag{56}$$

where

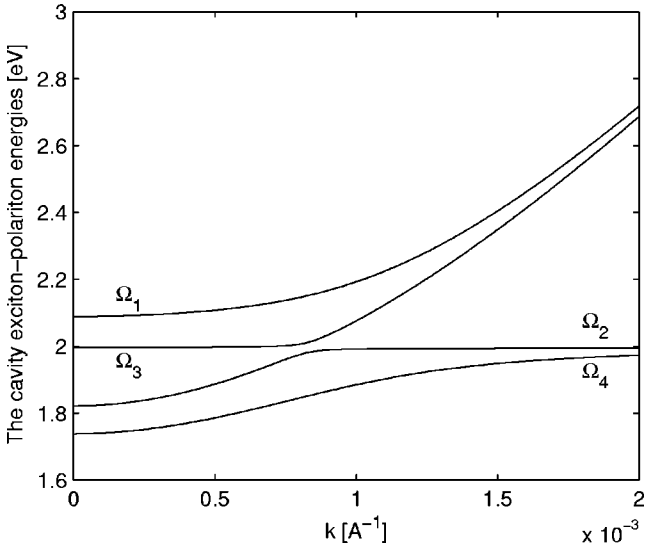

FIG. 8. The four cavity exciton-polariton energies vs in-plane wave vector k, for in-plane dipole moments, in the case of $W_a \gg W_b \sim \Delta_D$, where $\Delta_D = 0.01$ eV and $W_a = 0.15$ eV, $W_b = 0.015$ eV.

$$C_{\mathbf{k}a}^{1,2} = \pm \sqrt{\frac{\Delta_{\mathbf{k}}^{a} \pm \delta_{\mathbf{k}}^{a}}{2\Delta_{\mathbf{k}}^{a}}}, \quad C_{\mathbf{k}b}^{3,4} = \pm \sqrt{\frac{\Delta_{\mathbf{k}}^{b} \pm \delta_{\mathbf{k}}^{b}}{2\Delta_{\mathbf{k}}^{b}}},$$

$$C_{\mathbf{k}b}^{1,2} = 0, \quad C_{\mathbf{k}a}^{3,4} = 0, \tag{57}$$

and

$$X_{\mathbf{k}\lambda}^{1,2} = \frac{f_{\mathbf{k}\lambda}^{a}}{2\Delta_{\mathbf{k}}^{a}(\Delta_{\mathbf{k}}^{a} \pm \delta_{\mathbf{k}}^{a})}, \quad X_{\mathbf{k}\lambda}^{3,4} = \frac{f_{\mathbf{k}\lambda}^{b}}{2\Delta_{\mathbf{k}}^{b}(\Delta_{\mathbf{k}}^{b} \pm \delta_{\mathbf{k}}^{b})}, \tag{58}$$

and where we defined

$$\Delta_{\mathbf{k}}^{\nu 2} = \delta_{\mathbf{k}}^{\nu 2} + |f_{\mathbf{k}}^{\nu}|^2, \quad \delta_{\mathbf{k}}^{\nu} = \frac{\omega_{\nu}^{ex}(\mathbf{k}) - \omega_{\mathbf{k}}^{cav}}{2},$$

$$|f_{\mathbf{k}}^{\nu}|^2 = |f_{\mathbf{k}s}^{\nu}|^2 + |f_{\mathbf{k}p}^{\nu}|^2. \tag{59}$$

The inverse transformation is

$$B_{\mathbf{k}}^{\nu} = \sum_{r} C_{\mathbf{k}\nu}^{r*} A_{\mathbf{k}}^{r}, \quad a_{\mathbf{k}\lambda} = \sum_{r} X_{\mathbf{k}\lambda}^{r*} A_{\mathbf{k}}^{r}. \tag{60}$$

Each one of the four polariton branches is related to both cavity-mode polarizations, whereas the two polariton branches (1) and (2) are related to the (a) exciton branch, and the (3) and (4) polariton branches are related to the (b) exciton branch. Thus, in the case of in-plane dipole moments, and in the limit of long waves, the exciton-cavity-mode coupling does not mix the two exciton branches, (a) and (b).

2. General molecule dipole moments

In the case of general molecule dipole moments, we use the results of Sec. III B 2. This case, which is not treated in Ref. 9, leads to a mixing between the two exciton Davydov branches.

The coupling parameters between the exciton branches and the cavity modes, in terms of the orthogonal dipole moments, are given by

$$f_{\mathbf{k}\lambda}^{\nu} = iS(\mathbf{k}) \sum_{\alpha=\pm} R_{\nu}^{\alpha *}(\mathbf{k}) [\vec{\mu}_{\alpha} \cdot \mathbf{C}_{\lambda}(\mathbf{k})], \tag{61}$$

where $S(\mathbf{k})$ is as defined before in Eq. (43), and the functions $R_{\nu}^{\alpha *}(\mathbf{k})$ are given in Eqs. (34), which are the amplitude parameters of the orthogonal dipole moments in each exciton Davydov branch. We remind that the indexes $\alpha = \pm$ stand for the two orthogonal dipole moments, and $\nu = a, b$ for the two Davydov exciton branches. We consider only cavity modes with $(m=1)$. Furthermore, for the molecule transition dipole moments we choose a general case of $\vec{\mu}_1 = (\mu_1^x, \mu_1^y, \mu_1^z)$ and $\vec{\mu}_2 = (\mu_2^x, \mu_2^y, \mu_2^z)$, which yield the two general orthogonal dipole moments $\vec{\mu}_+ = (\mu_+^x, \mu_+^y, \mu_+^z)$ and $\vec{\mu}_- = (\mu_-^x, \mu_-^y, \mu_-^z)$. Substituting $\mathbf{C}_{\lambda}(\mathbf{k})$ from Eqs. (4) evaluated at $z=0$, and with the definitions of Eqs. (45) for the unit vectors, we get

$$f^{\nu}_{\mathbf{k}p} = \sqrt{1-\frac{k^2}{Q^2}}\{W^x_{\mathbf{k}\nu}\cos\phi + W^y_{\mathbf{k}\nu}\sin\phi\},$$

$$f^{\nu}_{\mathbf{k}s} = -i\{W^x_{\mathbf{k}\nu}\sin\phi - W^y_{\mathbf{k}\nu}\cos\phi\}, \tag{62}$$

where

$$W^x_{\mathbf{k}\nu} = S(\mathbf{k})\{R^{+*}_{\nu}(\mathbf{k})\mu^x_{+} + R^{-*}_{\nu}(\mathbf{k})\mu^x_{-}\},$$

$$W^y_{\mathbf{k}\nu} = S(\mathbf{k})\{R^{+*}_{\nu}(\mathbf{k})\mu^y_{+} + R^{-*}_{\nu}(\mathbf{k})\mu^y_{-}\}, \tag{63}$$

and Q is as defined in Eq. (44). In spite of the fact that the z component of the dipole moments does not couple to the $(m=1)$ cavity modes, when the slab is located at $z=0$, the z component of the dipole moment is included in the $R^{\alpha^*}_{\nu}(\mathbf{k})$ parameters of Eqs. (34) via the exciton dynamical matrix $V^{+-}(\mathbf{k},k_z)$.

By substituting Eqs. (62) in the relation of Eq. (51), in the long wave limit where $k \ll Q$, we get

$$\begin{aligned}&\{[\Omega_r(\mathbf{k}) - \omega^{ex}_a(\mathbf{k})][\Omega_r(\mathbf{k}) - \omega^{cav}_{\mathbf{k}}] - |W_{\mathbf{k}a}|^2\}\\ &\times\{[\Omega_r(\mathbf{k}) - \omega^{ex}_b(\mathbf{k})][\Omega_r(\mathbf{k}) - \omega^{cav}_{\mathbf{k}}] - |W_{\mathbf{k}b}|^2\}\\ &= |(W^{x*}_{\mathbf{k}a}W^x_{\mathbf{k}b} + W^{y*}_{\mathbf{k}a}W^y_{\mathbf{k}b})|^2,\end{aligned} \tag{64}$$

where

$$|W_{\mathbf{k}a}|^2 = |W^x_{\mathbf{k}a}|^2 + |W^y_{\mathbf{k}a}|^2,$$

$$|W_{\mathbf{k}b}|^2 = |W^x_{\mathbf{k}b}|^2 + |W^y_{\mathbf{k}b}|^2. \tag{65}$$

It is seen that the explicit dependence on ϕ has been canceled out, and we note that the small anisotropy effects contained in the R functions can be neglected in the long wavelength limit. Here, the right hand side of the relation is not negligible in the limit of long wave lengths. In the following we treat the two cases of small and large Davydov splitting compared to the Rabi splitting in the strong coupling regime. (*i*) *Small Davydov splitting*. As an example we will solve Eq. (64) in the limit of strong coupling between the excitons and the cavity modes, assuming that the Rabi splitting between the polariton branches is much bigger than the Davydov splitting between the exciton branches. Hence, in this limit we can assume that the two exciton branch energies are very close to each other. Therefore, we can assume that $\omega^{ex}_a(\mathbf{k}) \simeq \omega^{ex}_b(\mathbf{k}) = \omega^{ex}_0(\mathbf{k})$. The four polariton dispersion relations are

$$\Omega_{1,2,3,4}(\mathbf{k})\left[\frac{\omega^{ex}_0(\mathbf{k}) + \omega^{cav}_{\mathbf{k}}}{2}\right] \pm \sqrt{\mathcal{G}_{\pm}(\mathbf{k})}, \tag{66}$$

where

$$\begin{aligned}\mathcal{G}_{\pm}(\mathbf{k}) &= \frac{2\delta^2_{\mathbf{k}} + |W_{\mathbf{k}a}|^2 + |W_{\mathbf{k}b}|^2}{2}\\ &\pm \sqrt{\left(\frac{|W_{\mathbf{k}a}|^2 - |W_{\mathbf{k}b}|^2}{2}\right)^2 + |(W^{x*}_{\mathbf{k}a}W^x_{\mathbf{k}b} + W^{y*}_{\mathbf{k}a}W^y_{\mathbf{k}b})|^2},\end{aligned} \tag{67}$$

with the detuning $\delta_{\mathbf{k}} = [\omega^{ex}_0(\mathbf{k}) - \omega^{cav}_{\mathbf{k}}]/2$. In this case, the two exciton branches (a) and (b) are mixed with the two cavity-mode polarizations (s) and (p), where each polariton branch is a coherent superposition of both exciton branches and both cavity-mode polarizations.

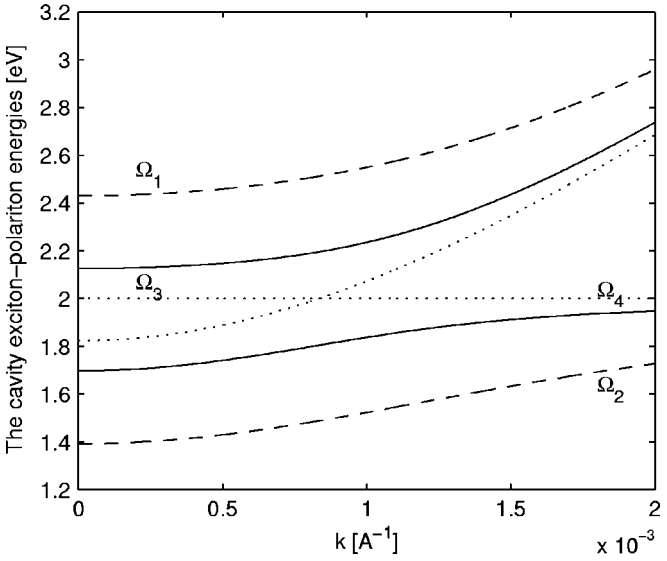

FIG. 9. The four cavity exciton-polariton energies vs in-plane wave vector k, for general dipole moments. The horizontal dotted line is the two Davydov exciton branches, where we assumed that they are very close to each other. The parabolic dotted line is the cavity-mode dispersion. The two Davydov exciton branches are strongly coupled with the cavity modes.

The four polariton dispersion branches are plotted in Fig. 9 for small wave vectors. The Ω_1 branch stands for $(++)$ of Eq. (66), Ω_2 for $(-+)$, Ω_3 for $(+-)$, and Ω_4 for $(--)$. As we assumed, the two Davydov exciton dispersions are very close to each other, and in the figure they coincide. For large wave vectors the branches Ω_1 and Ω_3 tend to the cavity mode dispersion, and the branches Ω_2 and Ω_4 tend to the exciton branch. For small wave vectors the branch Ω_3 is closer to the exciton one than the branch Ω_1; and the branch Ω_4 is closer to the cavity mode dispersion than the Ω_2 branch. These results are due to the following exciton cavity mode strong coupling parameters. The parameters $W^{x,y}_{\mathbf{k}\nu}$ of Eqs. (63) are assumed to be constants in the limit of long wave lengths, and the transition molecules dipole moments are chosen in such a way to ensure strong coupling parameters. For the case when the Davydov splitting is dominated by the exciton dynamical matrix $V^{+-}(\mathbf{k}k_z)$, from Eqs. (32) we have $|\Delta(\mathbf{k},k_z)| \sim |V^{+-}(\mathbf{k},k_z)|$, and from Eqs. (34) in the long wave limit, we get $R^+_a = R^-_a = R^-_b \approx 1/\sqrt{2}$ and $R^+_b \approx -1/\sqrt{2}$. These numbers, for example, are obtained by using the orthogonal dipole moments $\vec{\mu}_+ = \mu_0(-1,3,2)$ and $\vec{\mu}_- = \mu_0(5,5,-5)$, where $\mu_0 = 10\sqrt{\text{eV Å}^3}$. The two Davydov exciton branch energies at small wave vectors are $\hbar\omega^{ex}_a(\mathbf{k}) \simeq \hbar\omega^{ex}_b(\mathbf{k}) = 2$ eV. While the other parameters of the cavity are as for Fig. 4. As a result, we get large Rabi splitting relative to the Davydov splitting; the obtained values are: $W^x_a = 0.2$ eV, $W^x_b = 0.3$ eV, $W^y_a = 0.4$ eV, and $W^y_b = 0.1$ eV, which are used in Fig. 9.

As a second example, we consider the case with orthogonal dipole moments $\vec{\mu}_+ = (\mu^x_+, 0, 0)$ and $\vec{\mu}_- = (0, \mu^y_-, \mu^z_-)$. From

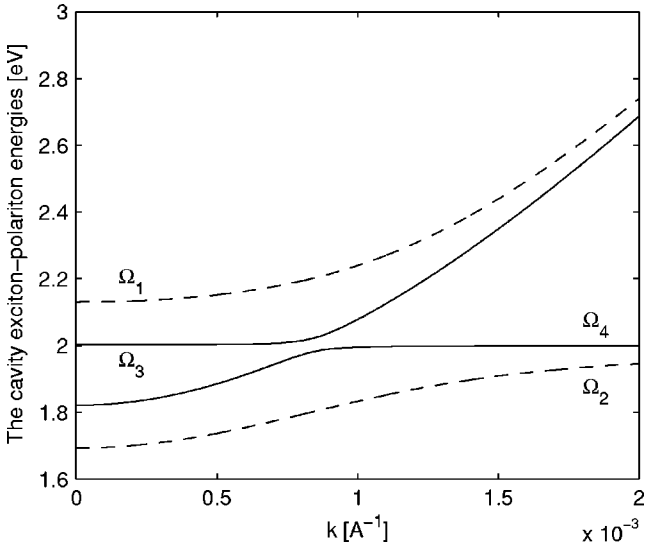

FIG. 10. The four cavity exciton-polariton energies vs in-plane wave vector k, for general dipole moments. The (a) exciton Davydov branch is with large Rabi splitting, and the (b) exciton Davydov branch is with small Rabi splitting.

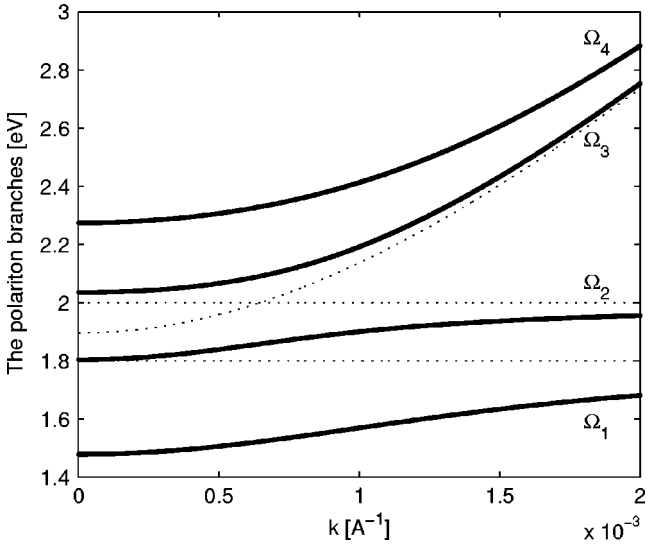

FIG. 11. The four cavity exciton-polariton energies vs in-plane wave vector k. The two horizontal dotted lines are for the two Davydov exciton branches. The parabolic dotted line is the cavity-mode dispersion.

Eqs. (17), we obtain $V^{+-}(\mathbf{k},k_z)=0$, then we have $R_a^+=R_b^-=1$ and $R_a^-=R_b^+=0$. Hence, Eqs. (63) yield $W_{\mathbf{k}a}^x=S(\mathbf{k})\mu_+^x$, $W_{\mathbf{k}b}^y=S(\mathbf{k})\mu_-^y$, and $W_{\mathbf{k}b}^x=W_{\mathbf{k}a}^y=0$. In this special case there is no mixing between the two exciton Davydov branches, which is similar to the in-plane dipole moment case. In Fig. 10 the four polariton branches are plotted, when the transition dipole moments are chosen in such a way that $\mu_+^x \gg \mu_-^y$. For the case of $\mu_+^x=20\sqrt{\text{eV Å}^3}$ and $\mu_-^y=2\sqrt{\text{eV Å}^3}$ we get that the (a) Davydov exciton branch is coupled with the cavity modes, with coupling parameter $W_a^x=0.2$ eV, while the (b) Davydov exciton branch is coupled with the cavity modes with coupling parameter $W_b^y=0.02$ eV. The result is that the Ω_1 and Ω_2 polariton branches have large Rabi splitting, but the Ω_3 and Ω_4 polariton branches have small Rabi splitting. As the Davydov branches are not mixed, the polariton dispersions in Fig. 10 are similar to that of Fig. 8.

(*ii*) *Large Davydov splitting*. Here, we consider the case when the Davydov splitting energy is from the order of the Rabi splitting energy in the strong coupling regime. The four polariton branches are a coherent superposition of the two exciton Davydov branches and the two cavity mode polarizations, as in Eqs. (56) here are rewritten as

$$A_{\mathbf{k}}^r = \alpha_{\mathbf{k}r}B_{\mathbf{k}}^a + \beta_{\mathbf{k}r}B_{\mathbf{k}}^b + \gamma_{\mathbf{k}r}a_{\mathbf{k}s} + \delta_{\mathbf{k}r}a_{\mathbf{k}p}, \tag{68}$$

where the coefficients $\alpha_{\mathbf{k}r}$, $\beta_{\mathbf{k}r}$, $\gamma_{\mathbf{k}r}$, and $\delta_{\mathbf{k}r}$ are the amplitudes of the (a) and (b) Davydov excitons, (s) and (p) polarization cavity modes in each polariton branch (r), respectively, and which obey $|\alpha_{\mathbf{k}r}|^2+|\beta_{\mathbf{k}r}|^2|+|\gamma_{\mathbf{k}r}|^2+|\delta_{\mathbf{k}r}|^2=1$. We solve the system numerically to get the four polariton dispersions, with the excitonic and the photonic weights in each polariton branch. The two exciton Davydov energies are chosen to be $\hbar\omega_a^{ex}=1.8$ eV and $\hbar\omega_b^{ex}=2$ eV. For the cavity we use the dielectric constant $\epsilon=4$, and the distance between the mirrors is $L=1635$ Å. The exciton-photon coupling parameters are $W_a^x=0.15$ eV, $W_a^y=0.3$ eV, $W_b^x=0.2$ eV, and $W_b^y=0.1$ eV. At $k=0$ the cavity dispersion falls between the two Davydov exciton branches. The four polariton branches are plotted in Fig. 11. The excitonic and photonic weights in each polariton branch are plotted in Figs. 12–15. It is seen that each polariton branch is a mix between the two Davydov excitons and the two cavity photon polarizations. For small in-plane wave vectors there is strong mixing between the two Davydov excitons in each polariton branch. At large in-plane wave vectors the two upper polariton branches, (3) and (4), tend to the cavity photon dispersion, the first lower polariton, (1), tend to the (a) Davydov exciton dispersion, and the second lower polariton, (2), tend to the (b) Davydov exciton dispersion.

For the case when the distance between the two cavity mirrors is $L=1900$ Å, where the cavity dispersion falls be-

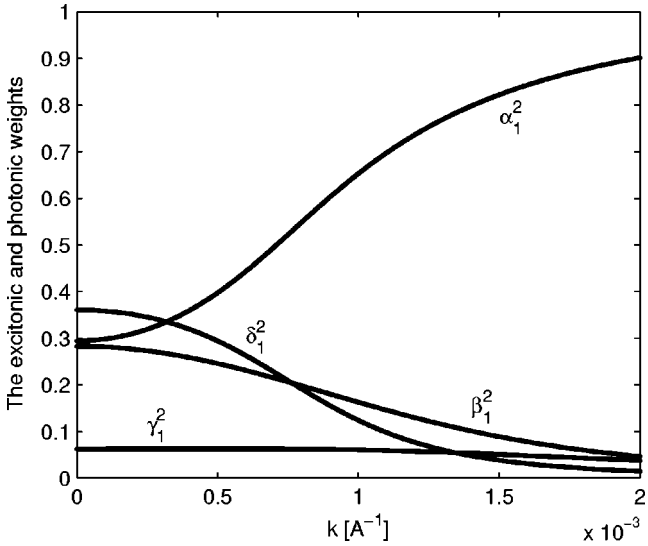

FIG. 12. The excitonic and photonic weights for the first polariton branch, which is Ω_1 in Fig. 11.

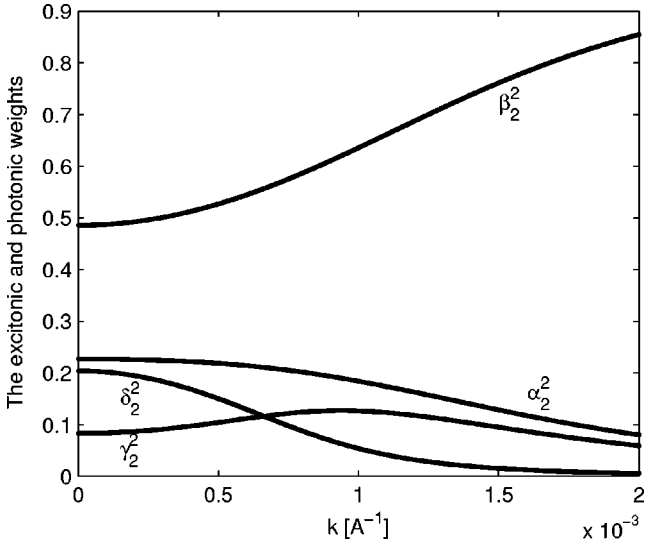

FIG. 13. The excitonic and photonic weights for the second polariton branch, which is Ω_2 in Fig. 11.

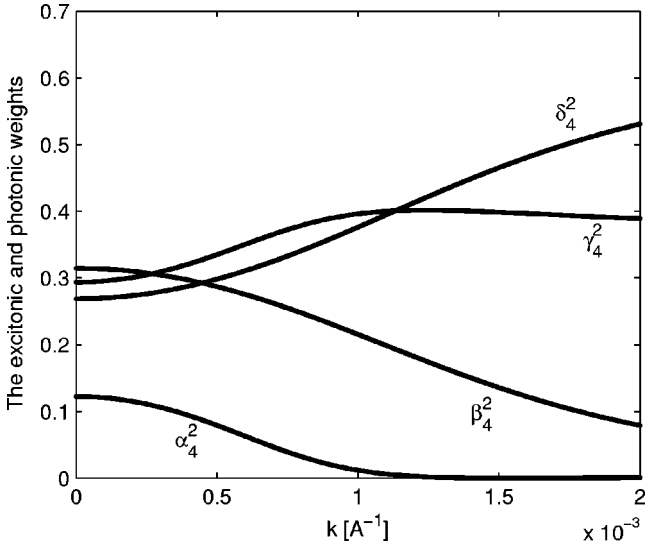

FIG. 15. The excitonic and photonic weights for the fourth polariton branch, which is Ω_4 in Fig. 11.

low the two Davydov dispersions at $k=0$, and by using the same numbers as above, the four polariton dispersions are plotted in Fig. 16.

V. TRANSMISSION, REFLECTION, AND ABSORPTION COEFFICIENTS FOR ANISOTROPIC ORGANIC CAVITIES

Up to this point, the discussion was limited to the case of a cavity with ideal mirrors, where the electromagnetic fields are confined inside the cavity. To observe the physical properties of the organic cavity, we need to couple the internal cavity fields with the external ones. One way to do this is by applying the quasimode formalism.[27] We assume nonideal cavity mirrors, which allow a coupling between the confined cavity modes and the external fields, to the left and the right sides of the cavity. The quasimode model is applicable only for a cavity with high quality mirrors.

We consider an organic cavity, where the optically resonant material is taken to be an anisotropic crystal slab. As discussed before, the excitons and the two cavity-mode polarizations, (*s*) and (*p*), are mixed together to produce the cavity polaritons. The absorption in the cavity medium is included phenomenologically by the decay of the system excitons into a heat reservoir, which describes the exciton finite lifetime. By applying the quasimode model, we can calculate the transmission, reflection, and absorption coefficients of the organic cavity for a given input field.

In general, the organic cavity Hamiltonian in terms of the system polaritons, is as given by Eq. (37). For the polariton

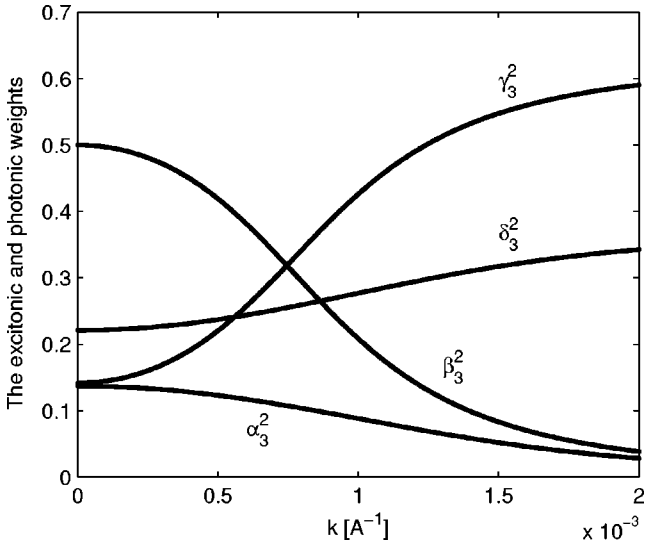

FIG. 14. The excitonic and photonic weights for the third polariton branch, which is Ω_3 in Fig. 11.

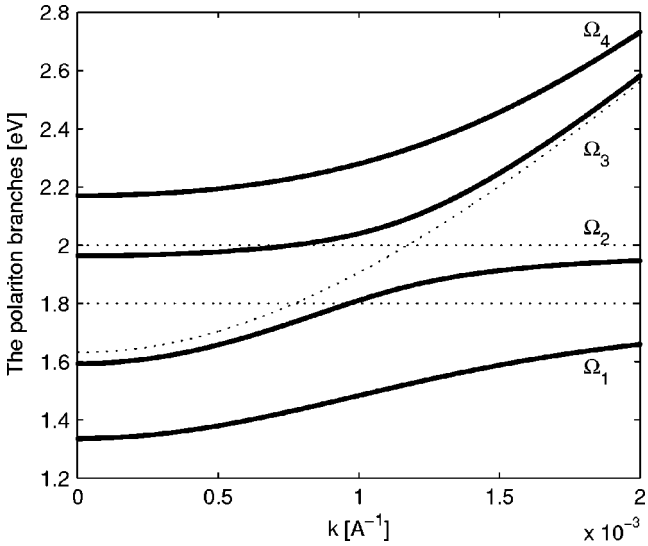

FIG. 16. The four cavity exciton-polariton energies vs in-plane wave vector *k*. The two horizontal dotted lines are for the two Davydov exciton branches. The parabolic dotted line is the cavity-mode dispersion.

operators $A^{r\dagger}_{\mathbf{k}}$, $A^{r}_{\mathbf{k}}$, and frequencies $\Omega_r(\mathbf{k})$, later we will use the results we obtained above for the two cases of organic crystal with one and two molecules per unit cell.

The continuum of external fields, to the left and the right sides of the cavity, are defined by the Hamiltonians

$$H_{FR} = \sum_{\mathbf{k}\lambda} \int d\omega_{\mathbf{k}} \hbar \omega_{\mathbf{k}} b^{\dagger}_{\mathbf{k}\lambda}(\omega_{\mathbf{k}}) b_{\mathbf{k}\lambda}(\omega_{\mathbf{k}}),$$

$$H_{FL} = \sum_{\mathbf{k}\lambda} \int d\omega_{\mathbf{k}} \hbar \omega_{\mathbf{k}} c^{\dagger}_{\mathbf{k}\lambda}(\omega_{\mathbf{k}}) c_{\mathbf{k}\lambda}(\omega_{\mathbf{k}}), \tag{69}$$

where $b^{\dagger}_{\mathbf{k}\lambda}(\omega_{\mathbf{k}})$, $b_{\mathbf{k}\lambda}(\omega_{\mathbf{k}})$, $[c^{\dagger}_{\mathbf{k}\lambda}(\omega_{\mathbf{k}}), c_{\mathbf{k}\lambda}(\omega_{\mathbf{k}})]$ are the creation and annihilation operators of an external mode at the right side (at the left side), with in-plane wave vector $\mathbf{k}$, polarization λ, and frequency $\omega_{\mathbf{k}}$, respectively. The cavity modes and the external fields, to the left and the right sides, are coupled via the nonideal cavity mirrors, by the coupling Hamiltonian

$$V = i\sum_{\mathbf{k}\lambda} \int d\omega_{\mathbf{k}} \hbar u(\omega_{\mathbf{k}}) [a_{\mathbf{k}\lambda} b^{\dagger}_{\mathbf{k}\lambda}(\omega_{\mathbf{k}}) - b_{\mathbf{k}\lambda}(\omega_{\mathbf{k}}) a^{\dagger}_{\mathbf{k}\lambda}],$$
$$+ i\sum_{\mathbf{k}\lambda} \int d\omega_{\mathbf{k}} \hbar v(\omega_{\mathbf{k}}) [a_{\mathbf{k}\lambda} c^{\dagger}_{\mathbf{k}\lambda}(\omega_{\mathbf{k}}) - c_{\mathbf{k}\lambda}(\omega_{\mathbf{k}}) a^{\dagger}_{\mathbf{k}\lambda}], \tag{70}$$

where $u(\omega_{\mathbf{k}})$, $[v(\omega_{\mathbf{k}})]$ is the coupling parameter of the right (left) side mirror. The coupling is between cavity modes and external modes with the same in-plane wave vectors and polarizations. The system can be treated for each in-plane wave vector $\mathbf{k}$ separately. The equations of motion for the external field operators, for a fixed $\mathbf{k}$, are given by

$$\frac{d}{dt} b_{\lambda}(\omega) = -i\omega b_{\lambda}(\omega) + u(\omega) \sum_{r} X^{r*}_{\lambda} A^{r},$$

$$\frac{d}{dt} c_{\lambda}(\omega) = -i\omega c_{\lambda}(\omega) + v(\omega) \sum_{r} X^{r*}_{\lambda} A^{r}, \tag{71}$$

and for the polariton operators

$$\frac{d}{dt} A^{r} = -i\Omega_r A^{r} - \sum_{\lambda} \int d\omega X^{r}_{\lambda} \{u(\omega) b_{\lambda}(\omega) + v(\omega) c_{\lambda}(\omega)\}, \tag{72}$$

where we dropped $\mathbf{k}$. The cavity-mode operators have been represented in terms of the polariton operators by $a_{\lambda} = \Sigma_r X^{r*}_{\lambda} A^{r}$. For simplicity, we assume two similar mirrors, that is $u(\omega) = v(\omega)$. We take $u(\omega)$ to be an independent function of frequency, over a frequency band which includes the relevant organic cavity frequencies. Namely, we assume $u^2(\omega) = \gamma/2\pi$, which is a good approximation for high quality mirrors, where γ is related to the mirror reflectivity ($\gamma \propto 1-R$).[27]

We solved the above system of Eqs. (71) and (72), for a given initial external input field from the right side, with a fixed polarization, to get the external output fields from the left and the right sides.[28] Due to the anisotropic organic material, the output fields contain the two polarizations, (s) and (p), although the input field is with one polarization only, (s) or (p). From the solutions we derive the transmission, reflection, and absorption coefficients.

The absorption of the medium is included phenomenologically, by replacing the exciton frequency with a complex one, namely $\omega^{ex} \rightarrow \omega^{ex} - i\Gamma$, where Γ is the nonradiative damping rate of the excitons. In the case of more than one exciton branch, as the case for crystals with two molecules per unit cell where two Davydov exciton branches are obtained, in principle there are different damping rates Γ_{ν} for each exciton branch ν. Another approach to include the system dissipations phenomenologically,[29] which is applicable in the strong coupling regime when the exciton damping rate is smaller than the Rabi splitting, is by making the replacement $\Omega_r \rightarrow \Omega_r - i\Gamma_r$, where Γ_r is the damping rate of the rth polariton branch. These damping terms stem from the damping of the excitonic part of the polaritons. For example, in the case of organic cavity with one molecules per unit cell, the damping rates for the three polariton branches, ($r=1,2,3$), are $\Gamma_r = |C^r|^2 \Gamma$, where the $|C^r|^2$ parameters describe the excitonic weights in each polariton branch, and which are defined in Eqs. (40). While the latter approach would also be applicable for our system, in the following we use the former approach.

In the following we give the transmission, reflection, and absorption coefficients, for the two cases of (s) and (p) input fields. The coefficients are given in terms of the organic cavity matrix

$$\Lambda_{\lambda\mu} = \sum_{r} \frac{X^{r}_{\lambda} X^{r*}_{\mu}}{(\omega - \Omega_r)}. \tag{73}$$

(i) For the case of (s) polarized external input field from the right side, the reflection and transmission coefficients are

$$T^{(s)}_{s} = \frac{\gamma^2 |i\Lambda_{ss} + \gamma(\Lambda_{sp}\Lambda_{ps} - \Lambda_{ss}\Lambda_{pp})|^2}{|D|2},$$

$$T^{(s)}_{p} = R^{(s)}_{p} = \frac{\gamma^2 |\Lambda_{sp}|^2}{|D|^2}, \quad R^{(s)}_{s} = \frac{|1 + i\gamma\Lambda_{pp}|^2}{|D|^2}, \tag{74}$$

where

$$|D|^2 = |1 - \gamma^2 \Lambda_{pp}\Lambda_{ss} + \gamma^2 \Lambda_{sp}\Lambda_{ps} + i\gamma(\Lambda_{ss} + \Lambda_{pp})|^2. \tag{75}$$

The absorption coefficient, $A^{(s)}$, is obtained from the relation

$$T^{(s)}_{s} + T^{(s)}_{p} + R^{(s)}_{s} + R^{(s)}_{p} + A^{(s)} = 1. \tag{76}$$

Although the input field is (s) polarized, the organic material gives rise also to (p) polarized transmitted and reflected fields. The (p) polarized reflection and transmission coefficients are equal, this being due to the mirrors similarity.

(ii) For the case of (p) polarized external input field from the right side, the reflection and transmission coefficients are

$$T^{(p)}_{p} = \frac{\gamma^2 |i\Lambda_{pp} + \gamma(\Lambda_{sp}\Lambda_{ps} - \Lambda_{ss}\Lambda_{pp})|^2}{|D|^2},$$

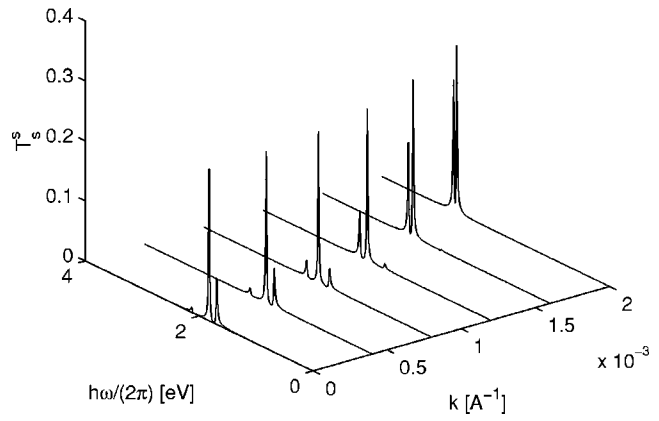

FIG. 17. The (*s*) polarized field transmission $T_s^{(s)}$ vs wave vector *k*, for (*s*) polarized input field, in the case of crystals with one molecule per unit cell.

$$T_s^{(p)} = R_s^{(p)} = \frac{\gamma^2|\Lambda_{ps}|^2}{|D|^2}, \quad R_p^{(p)} = \frac{|1 + i\gamma\Lambda_{ss}|^2}{|D|^2}. \tag{77}$$

The absorption parameter, $A^{(p)}$, is obtained from the relation

$$T_s^{(p)} + T_p^{(p)} + R_s^{(p)} + R_p^{(p)} + A^{(p)} = 1. \tag{78}$$

Although the input field is (*p*) polarized, the organic material gives rise also to (*s*) polarized transmitted and reflected fields. The (*s*) polarized reflection and transmission coefficients are equal, this being due to the mirrors similarity.

For the case of organic cavity with one molecule per unit cell, we obtained in Sec. IV A three polariton branches ($r=1, 2, 3$), with the frequencies Ω_r, which are given in Eqs. (38), and the X_λ^r parameters are given in Eqs. (40). We concentrate in the case of (*s*) polarized input field from the cavity right side. In the following figures we used the organics typical numbers, that was used in Fig. 4. We consider the case of the transition dipole moment $\vec{\mu}=(\mu_x, 0, \mu_z)$. The exciton-cavity mode coupling parameters are defined in Eqs.

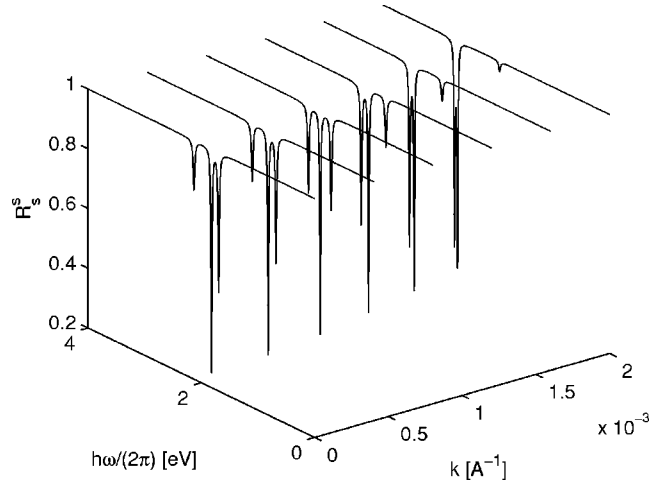

FIG. 18. The (*s*) polarized field reflection $R_s^{(s)}$ vs wave vector *k*, for (*s*) polarized input field, in the case of crystals with one molecule per unit cell.

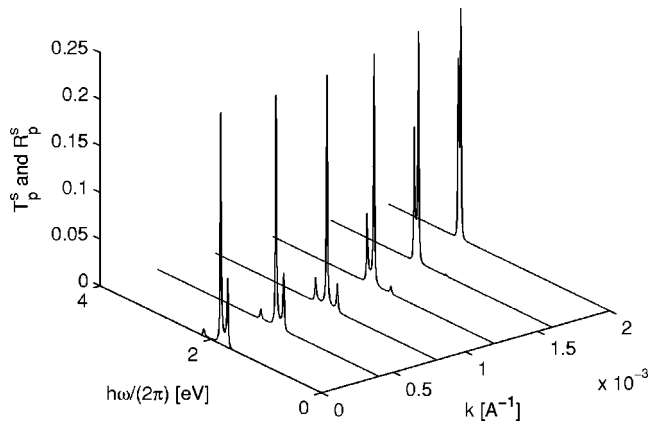

FIG. 19. The (*p*) polarized field transmission and reflection, $T_p^{(s)}$ and $R_p^{(s)}$, vs wave vector *k*, for (*s*) polarized input field, in the case of crystals with one molecule per unit cell.

(46) for the ($m=1$) cavity modes, where the angle ϕ is between the in-plane wave vector $\mathbf{k}$ and the *x* axis. The parameter $W(\mathbf{k})$ is assumed to be a constant for the limit of small wave vectors, with $S \approx 0.02\sqrt{\text{eV}/\text{Å}^3}$, and for $\mu_x = 10\sqrt{\text{eV Å}^3}$ we have $W=0.2$ eV. The cavity mirror damping rate, which is derived from the mirrors reflectivity, is estimated to be $\hbar\gamma=0.01$ eV, and the exciton damping rate is $\hbar\Gamma=0.02$ eV. For the direction with $\phi=\pi/4$, Eqs. (74)–(76) are plotted in Figs. 17–20. The (*s*) polarized field transmission $T_s^{(s)}$ is plotted in Fig. 17, for different in-plane wave vectors *k*. We have transmission at resonance points with the polariton branches. Large transmitted field is obtained from regions where the polariton branch is more photonic than excitonic; this is for the lower branch to the left of the exciton-cavity mode intersection point, and for the upper branch to the right, plus the purely photonic branch. The (*s*) polarized field reflection $R_s^{(s)}$ is plotted in Fig. 18. The reflection dip at resonance points where the polariton branch is more photonic is deeper than where the polariton branch is more excitonic. Around the intersection point we have three resonance points corresponding to the three polariton branches. In Fig. 19 the (*p*) polarized field transmission and reflection, $T_p^{(s)}$ and $R_p^{(s)}$, are plotted, note that in this case the reflection and transmission

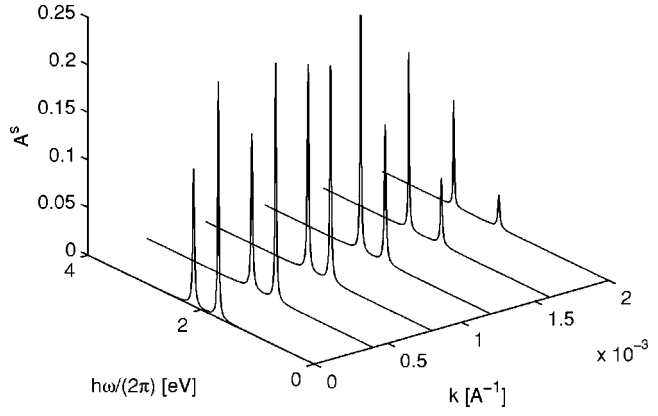

FIG. 20. The absorption $A^{(s)}$ vs wave vector *k*, for (*s*) polarized input field, in the case of crystals with one molecule per unit cell.

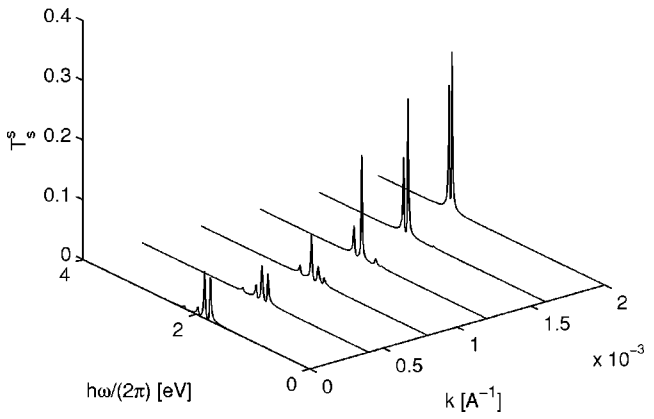

FIG. 21. The (s) polarized field transmission $T_s^{(s)}$ vs wave vector k, for (s) polarized input field, in the case of crystals with two molecules per unit cell.

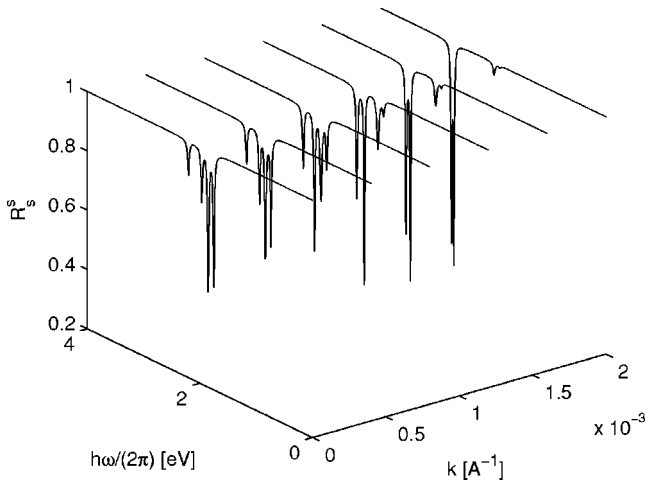

FIG. 22. The (s) polarized field reflection $R_s^{(s)}$ vs wave vector k, for (s) polarized input field, in the case of crystals with two molecules per unit cell.

are equal. Here, the transmitted and reflected fields are strong at resonance points where the polariton branches correspond to a significant mixing of both polarizations. The absorption $A^{(s)}$ are plotted in Fig. 20. The absorption is strong at resonance points with the polariton branches in the regions where both the photonic and the excitonic components are significant. This is due to the fact that in these regions there is more penetration of the external field into the cavity than in the regions where the polariton states are predominantly excitonic. We have absorption resonance points at the upper and lower polariton branches, and there is no absorption from the pure photonic polariton branch. Good agreement is obtained between the present $(s)-(p)$ polarization mixing results and those of Ref. 10, which are derived in applying a macroscopic dielectric theory, by using the (4×4) transfer matrix formalism, where a thin slab of oriented molecular aggregates is considered as an uniaxial organic material, and the optical axis is determined by the orientation of the transition dipole moment.

In a direction with $\phi=\pi/2$, we have $f_{\mathbf{k}s}=iW(\mathbf{k})$ and $f_{\mathbf{k}p}=0$, then $\Lambda_{sp}=\Lambda_{ps}=\Lambda_{pp}=0$, where we get

$$T_s^{(s)}=\frac{\gamma^2|i\Lambda_{ss}|^2}{|D|^2},\quad R_s^{(s)}=\frac{1}{|D|^2},\quad T_p^{(s)}=R_p^{(s)}=0, \qquad (79)$$

with $|D|^2=|1+i\gamma\Lambda_{ss}|^2$. There are no mixing between the two photon polarizations. Two resonance points will appear in the transmission, reflection, and absorption spectra at each in-plane wave vector. This thing is obtained due the fact that only the (s) polarized cavity photons are coupled with the excitons. For the case with $\phi=0$, in the long wave limit, we have $f_{\mathbf{k}p}\approx W(\mathbf{k})$ and $f_{\mathbf{k}s}=0$. For (s) polarized input fields the cavity photon polarization is orthogonal the transition dipole moments. Therefore, the obtained spectra are identical to that of empty cavity, where for each in-plane wave vector we get a single resonance point at the cavity frequency.

For an organic cavity with two molecules per unit cell, and with in-plane dipole moments, we obtained in Sec. IV B 1 four polariton branches $(r=1, 2, 3, 4)$, with the frequencies Ω_r, which are given in Eqs. (55), and where the X_λ^r parameters are given in Eqs. (58). We assume that the two exciton branches have the same damping rates $\Gamma_a=\Gamma_b=\Gamma$. Also here we concentrate in the case of (s) polarized input field from the cavity right side. In the following figures we used $\hbar\omega_a^{ex}=2.1$ eV and $\hbar\omega_b^{ex}=1.9$ eV, with the Davydov splitting of $\Delta_D=0.2$ eV. As in the one molecule per unit cell case, the distance between the cavity mirrors is $L=1700$ Å, and the cavity medium dielectric constant is $\epsilon=4$. We consider the case with orthogonal transition dipole moments of $\vec{\mu}_+=\mu_x^+\hat{\mathbf{x}}$ and $\vec{\mu}_-=\mu_y^-\hat{\mathbf{y}}$. The two exciton branches and the two cavity mode polarizations coupling parameters are defined in Eqs. (53) for the $(m=1)$ cavity modes, whereas above the angle ϕ is between the in-plane wave vector $\mathbf{k}$ and the x axis. The parameters $W_a(\mathbf{k})$ and $W_b(\mathbf{k})$, which appear in the polariton dispersions of Eqs. (55), are assumed to be constants in the limit of small wave vectors, with $S\approx0.02\sqrt{\text{eV/Å}^3}$. For $\mu_x^+=10\sqrt{\text{eV Å}^3}$ and $\mu_x^-=5\sqrt{\text{eV Å}^3}$, we have $W_a=0.2$ eV and $W_b=0.1$ eV. The cavity mirror damping rate is taken to be $\hbar\gamma=0.01$ eV, and the exciton damping rate is $\hbar\Gamma=0.03$ eV. In the direction of $\phi=\pi/4$ the results of Eqs. (74)–(76) are plotted in Figs. 21–24. The (s) polarized field transmission

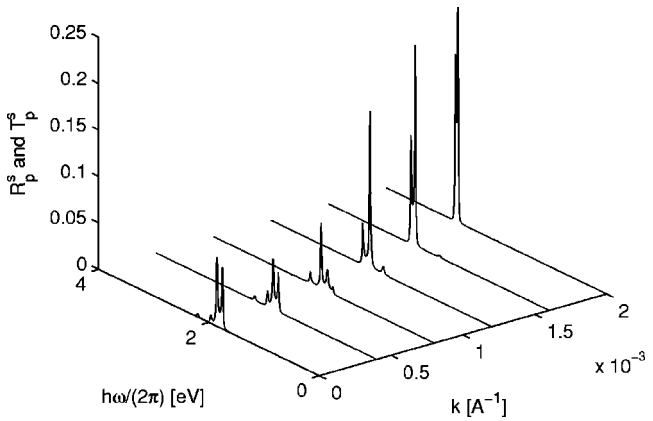

FIG. 23. The (p) polarized field transmission and reflection, $T_p^{(s)}$ and $R_p^{(s)}$, vs wave vector k, for (s) polarized input field, in the case of crystals with two molecules per unit cell.

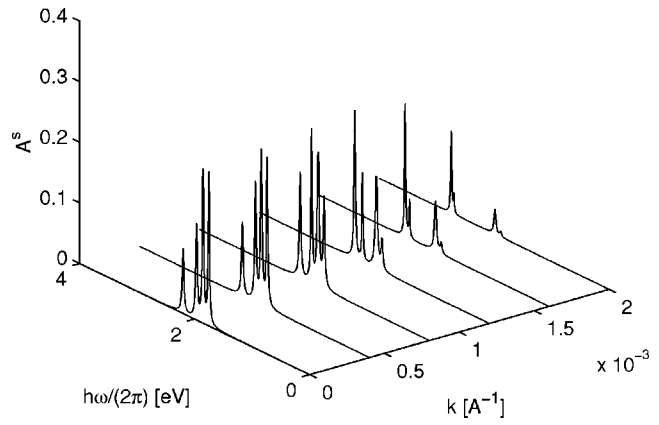

FIG. 24. The absorption $A^{(s)}$ vs wave vector k, for (s) polarized input field, in the case of crystals with two molecules per unit cell.

$T_s^{(s)}$ is plotted in Fig. 21, for different in-plane wave vectors k. Four resonance peaks appear at the four polariton dispersions. The transmission from regions of photonic like polariton dispersion is larger than that of excitoniclike ones. The (s) polarized field reflection $R_s^{(s)}$ is plotted in Fig. 22. Four reflection dips are obtained at resonances with the four polariton dispersions. The reflection dips at resonances with the polariton dispersions at the photoniclike regions are deeper than that at the excitoniclike ones. In Fig. 23 the (p) polarized field transmission and reflection, $T_p^{(s)}$ and $R_p^{(s)}$, are plotted, note that in this case the reflection and transmission are equal. Four reflection and transmission peaks appear around the intersection point corresponding to the four polariton branches. Large transmission is obtained at resonances with the four polariton dispersions where polarization mixing is large. The absorption $A^{(s)}$ are plotted in Fig. 24. Here, four absorption peaks are present at resonances with the four polariton branches.

In all of the above spectra we assumed equal exciton nonradiative damping rates for both Davydov branches. For example the reflection spectrum of the (s) polarized field, that appears in Fig. 22, is replotted in Fig. 25 for in-plane wave vector $q=10^{-4}$ Å^{-1}, and damping rates of $\hbar\Gamma_a=\hbar\Gamma_b=0.05$ eV. With in-plane dipole moments, no mixing between the two Davydov branches exists in the formation of the polaritons. Then changing the damping rate of one Davydov branch will affect only the width of dips at resonance with polaritons that are related to this Davydov branch. In Fig. 26 the above reflection spectrum is plotted in the case of two different damping rates, which are $\hbar\Gamma_a=0.05$ eV and $\hbar\Gamma_b=0.005$ eV. It is seen that significant changes are obtained at the polariton dips which are related to the (b) Davydov branch.

As the other side, in the case of general dipole moments with z components, from the results of Sec. IV B 2, we get that the two exciton Davydov branches are mixed in the formation of polaritons. Hence, we expect smaller changes in

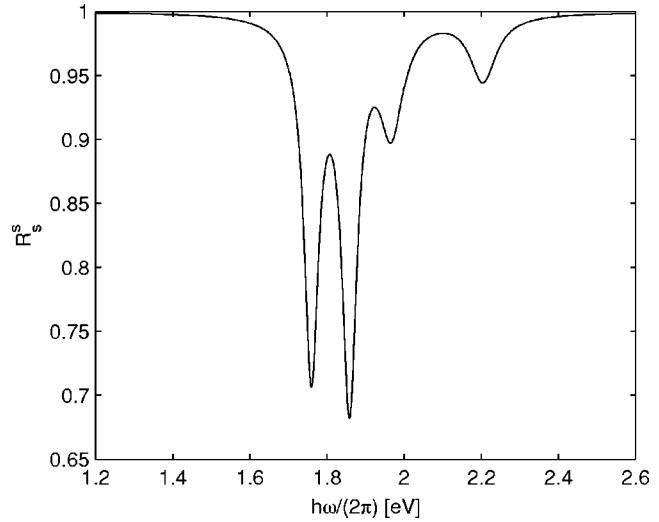

FIG. 25. The (s) polarized field reflection $R_s^{(s)}$ vs wave vector k, for (s) polarized input field. In the case of $\hbar\Gamma_a=\hbar\Gamma_b=0.05$ eV.

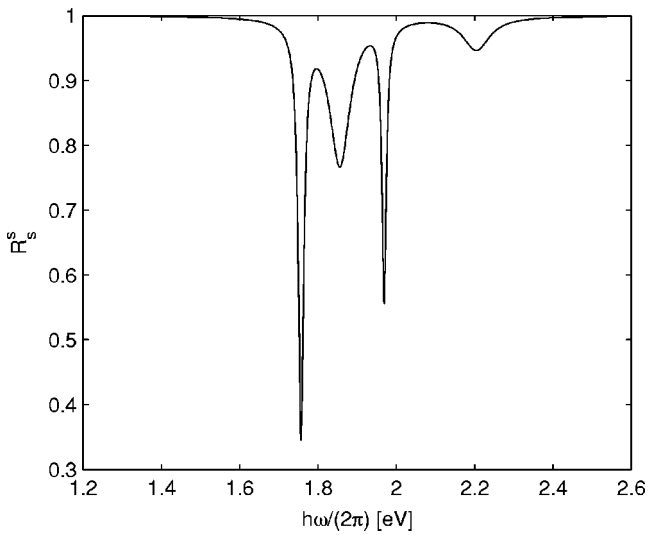

FIG. 26. The (s) polarized field reflection $R_s^{(s)}$ vs wave vector k, for (s) polarized input field, in the case of $\hbar\Gamma_a=0.05$ eV and $\hbar\Gamma_b=0.005$ eV.

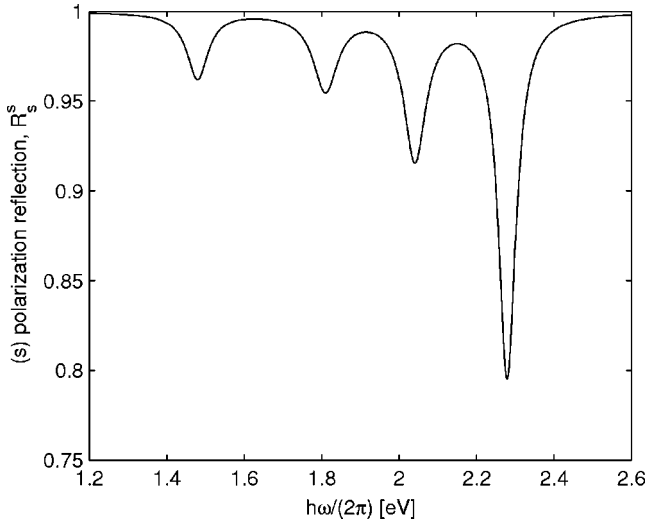

FIG. 27. The (s) polarized field reflection $R_s^{(s)}$ vs wave vector k, for (s) polarized input field. In the case of $\hbar\Gamma_a=\hbar\Gamma_b=0.05$ eV.

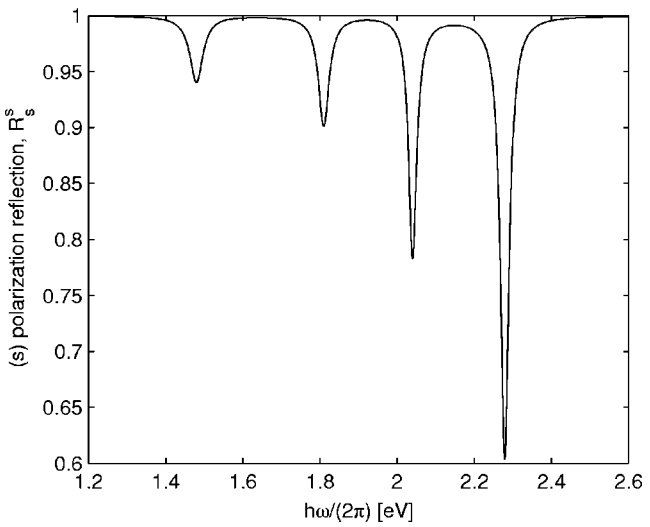

FIG. 28. The (s) polarized field reflection $R_s^{(s)}$ vs wave vector k, for (s) polarized input field, in the case of $\hbar\Gamma_a=0.05$ eV and $\hbar\Gamma_b=0.005$ eV.

the spectra by considering different damping rates for the two Davydov branches. The reflection spectrum of the (s) polarized field from an organic cavity, that is described by the polariton dispersions of Fig. 11, is plotted in Fig. 27, at the in-plane wave vector $q=10^{-4}$ Å^{-1}, and for the case of damping rates of $\hbar\Gamma_a=\hbar\Gamma_b=0.05$ eV. In Fig. 28 the same reflection spectrum is replotted for two different damping rates, which are $\hbar\Gamma_a=0.05$ eV and $\hbar\Gamma_b=0.005$ eV. No significant differences are obtained in this case, all reflection dips remaining of similar width, as opposed to Fig. 26.

VI. CONCLUSIONS

We have developed a microscopic theory for Frenkel-exciton polaritons in organic microcavities in the strong coupling regime. The Frenkel exciton states in an organic crystal slab with one or two molecules per unit cell and general dipole orientations have been presented and used to obtain the cavity polariton states calculating their coupling to the cavity photon modes microscopically. The dispersion curves of the organic cavity polaritons we calculate reproduce and extend the results previously derived within the macroscopical approach.[9] In the most general case, each one of the four cavity polariton branches is a coherent superposition of both Davydov exciton bands and both cavity mode polarizations.

Using the quasimode approach to couple the cavity polariton states to the continuum of external photons, we have then calculated the linear optical response spectra of the organic microcavity. These results reproduce and extend those previously obtained through a (4×4) transfer matrix formalism employing a phenomenological uniaxial dielectric tensor appropriate for the simplest case of one molecule per unit cell.[10] Aside from the higher number of cavity polariton branches involved, the spectra of the organic microcavity show a mixing between TM and TE polarizations which does not occur in the usual inorganic microcavities made of isotropic semiconductors.

The formalism presented here can also be used to consider more complex microcavity configurations containing several layers of different organic materials.

ACKNOWLEDGMENTS

H.Z. gratefully acknowledges the support of the European Commission via the 5th Framework Research Training Network HPRN-CT-2002-00315 "*The physics of hybrid organic-inorganic heterostructures for photonics and telecommunications*" (HYTEC). We would like to thank Vladimir Agranovich, and Franco Bassani for very fruitful discussions.

[1] *Electron and Photon Confinement in Semiconductor Nanostructures*, edited by B. Deveaud and A. Quattropani (CL Course of Enrico Fermi School of Physics, Bologna, 2002); *Organic Nanostructures: Science and Applications*, edited by V. M. Agranovich and G. C. La Rocca (CXLIX Course of Enrico Fermi School of Physics, Bologna, 2001); *Electronic Excitations in Organic Based Nanostructures*, Thin Films and Nanostructures 31, edited by V. M. Agranovich and G. F. Bassani (Elsevier, San Diego, 2003).

[2] C. Weisbuch, M. Nishioka, A. Ishikawa, and Y. Arakawa, Phys. Rev. Lett. **69**, 3314 (1992).

[3] G. Khitrova, H. M. Gibbs, F. Jahnke, M. Kira, and S. W. Koch, Rev. Mod. Phys. **71**, 1591 (1999); M. S. Skolnick, T. A. Fisher, and D. M. Whittaker, Semicond. Sci. Technol. **13**, 645 (1998); *Microcavities and Photonic Bandgaps: Physics and Applications*, edited by C. Weisbuch and J. G. Rarity (Kluwer, Dordrecht, 1996); A. Kavokin and G. Malpuech, Cavity Polaritons, *Thin Films and Nanostructures* 32 (Elsevier, San Diego, 2003).

[4] V. Agranovich, H. Benisty, and C. Weisbuch, Solid State Commun. **102**, 631 (1997).

[5] D. G. Lidzey, D. D. C. Bradley, M. S. Skolnik, T. Virgili, S. Walker, and D. M. Whittaker, Nature (London) **395**, 53 (1998).

[6] D. G. Lidzey, D. D. C. Bradley, T. Virgili, A. Armitage, M. S. Skolnick, and S. Walker, Phys. Rev. Lett. **82**, 3316 (1999); A. I. Tartakovskii, M. Emam-Ismail, D. G. Lidzey, M. S. Skolnick, D. D. C. Bradley, S. Walker, and V. M. Agranovich, Phys. Rev. B **63**, 121302(R) (2001); P. A. Hobson, W. L. Barnes, D. G. Lidzey, G. A. Gehring, D. M. Whittaker, M. S. Skolnik, and S. Walker, Appl. Phys. Lett. **81**, 3519 (2002); V. M. Agranovich, M. Litinskaia, and D. G. Lidzey, Phys. Rev. B **67**, 085311 (2003).

[7] S. Forrest, Chem. Rev. (Washington, D.C.) **97**, 1793 (1997).

[8] V. M. Agranovich, Sov. Phys. JETP **37**, 307 (1960); V. M. Agranovich, Sov. Phys. Solid State **3**, 592 (1961).

[9] M. Litinskaya, P. Reineker, and V. M. Agranovich, Phys. Status Solidi A **201**, 646 (2004).

[10] D. B. Balagurov and G. C. La Rocca, Phys. Status Solidi C **1**, 518 (2004).

[11] M. Schubert, Phys. Rev. B **53**, 4265 (1996).
[12] A. S. Davydov, *Theory of Molecular Excitons* (Plenum, New York, 1971).
[13] M. Born and E. Wolf, *Principles of Optics* (Plenum, Oxford, 1980).
[14] G. Panzarini, L. C. Andreani, A. Armitage, D. Baxter, M. S. Skolnick, N. V. Astratov, J. S. Roberts, A. V. Kavokin, M. R. Vladimirova, and M. A. Kaliteevski, Phys. Rev. B **59**, 5082 (1999); R. F. Oulton, N. Takada, J. Koe, P. N. Stavrinou, and D. D. C. Bradley, Semicond. Sci. Technol. **18**, S419 (2003).
[15] C. C. Tannoudji, J. Dupont Roc, and G. Grynberg, *Photons and Atoms: Introduction to Quantum Electrodynamics* (Wiley, New York, 1989).
[16] M. Pope and C. E. Swenberg, *Electronic Properties in Organic Crystals and Polymers* (Oxford University Press, New York, 1999); E. A. Silinsh, *Organic Molecular Crystals: Their Electronic States* (Springer-Verlag, Berlin, 1980).
[17] J. Knoester and V. M. Agranovich, Electronic Excitations in Organic Based Nanostructures, *Thin Films and Nanostructures* 31, edited by V. M. Agranovich and G. F. Bassani (Elsevier, San Diego, 2003).
[18] M. R. Philpott, J. Chem. Phys. **60**, 1410 (1974); M. R. Philpott, Phys. Rev. B **12**, 5381 (1975).
[19] V. M. Agranovich, and B. S. Toshich, Sov. Phys. JETP **26**, 104 (1968).
[20] V. M. Agranovich and A. M. Kamchatnov, Electronic Excitations in Organic Based Nanostructures, *Thin Films and Nanostructures* 31, edited by V. M. Agranovich and G. F. Bassani (Elsevier, San Diego, 2003).
[21] M. Born and K. Huang, *Dynamical Theory of Crystal Lattice*, (Clarendon, Oxford, 1954); M. H. Cohen and F. Keffer, Phys. Rev. **99**, 1128 (1955).
[22] H. Benson and D. L. Mills, Phys. Rev. **178**, 839 (1969).
[23] I. S. Gradshteyn, I. M. Ryzhik, A. Jeffrey, and D. Zwillinger, *Table of Integrals, Series, and Products* (Academic Press, San Diego, 2000).
[24] R. Fuchs and K. L. Kliewer, Phys. Rev. **140**, 2076 (1965).
[25] M. R. Philpott, J. Chem. Phys. **54**, 111 (1971).
[26] L. C. Andreani and F. Bassani, Phys. Rev. B **41**, 7536 (1990); L. C. Andreani, *Confined Electrons and Photons: New Physics and Applications*, edited by E. Burstein and C. Weisbuch (Plenum, New York, 1995).
[27] V. Savona, C. Piermarocchi, A. Quattropani, P. Schwendimann, and F. Tassone, Phase Transitions **68**, 169 (1999).
[28] M. J. Collett and C. W. Gardiner, Phys. Rev. A **30**, 1386 (1984).
[29] P. Kinsler and D. M. Whittaker, Phys. Rev. B **54**, 4988 (1996).